An integrated fertilizer driven forward osmosis- renewables powered membrane distillation system for brackish water desalination: a combined experimental and theoretical approach.

Wafa Suwaileh[a], Daniel Johnson[a], Daniel Jones[b], Nidal Hilal[a,c]

[a]*Centre for Water Advanced Technologies and Environmental Research (CWATER), College of Engineering, Swansea University, Swansea, SA1 8EN, UK*

[b] *Energy Safety Research Institute, Swansea University, Bay Campus, Swansea, SA1 8EN, UK*

[c]*NYUAD Water Research Center, New York University Abdu Dhabi, Abu Dhabi, United Arab Emirates*

Abstract

Utilization of an integrated forward osmosis-solar powered membrane distillation system can provide a promising method for brackish water desalination. In this study, the brackish water feed and fertilizer draw solutions were operated in a forward osmosis process to generate irrigation water for agriculture. Forward osmosis was also selected as membrane distillation pre-treatment to avoid fouling and wetting of the membrane distillation membrane. Subsequently, the diluted draw solutions were treated in the membrane distillation system to recover the initial osmotic pressure and to obtain a final distillate permeate. The experimental results revealed that the modified forward osmosis membrane exhibited slightly better performance in terms of maximum water flux, minimum reverse solute flux and high water recovery of 53.5%. In the membrane distillation process, an optimum water flux of about 5.7 L/m^2. hr and high rejection rate of about 99.55 % were achieved at an optimum temperature of 60 ^{o}C. Modelling was applied to investigate the feasibility of using a solar collector to power the membrane distillation system and hence limit energy costs. By using renewable energy, we calculate that the energy consumption of the hybrid system could be reduced by 67%. Membrane distillation-solar powered system can achieve optimum energy consumption recoded as 1.1 kWh. We concluded that the diluted fertilizer draw solution can be used as an irrigation water after further dilution by an available water source. By using forward osmosis prior to membrane distillation process, the membrane distillation membrane showed less fouling and wetting leading to excellent rejection rate and acceptable distillate permeate. The energy consumption of the forward osmosis-solar powered membrane distillation system was lower than that for reverse osmosis stand-alone system. The findings of this work could be used to develop guidelines for the optimal design of industrial forward osmosis-membrane distillation system.

Key words

Water desalination, forward osmosis, membrane distillation, modelling, optimization.

List of abbreviations

FO	Forward osmosis
ICP	Internal concentration polarization
IP	Interfacial polymerization process
UF	Ultrafiltration
NF	Nanofiltration
MD	Membrane distillation
MSF	Multistage flash
MED	Multiple-effect distillation
RO	Reverse osmosis
SEC	Specific energy consumption
BWRO	Brackish water reverse osmosis
SWRO	Seawater reverse osmosis
ED	Electrodialysis
Na_2SO_4	Sodium sulfate
$MgSO_4$	Magnesium sulfate
NaCl	Sodium chloride
DCMD	Direct contact membrane distillation
$TrOC_s$	Trace organic contaminants
EDTA-2Na	Ethylenediaminetetraacetic acid disodium salt
PES	Polyethersulfone
CMCNA	Sodium carboxymethyl cellulose
PDADMAC	Poly (diallyl dimethyl ammonium chloride)
PSS	Poly (sodium 4- styrenesulfonate)
PVDF	Polyvinylidene fluoride
LEP	Liquid entry pressure
DI water	Deionized water

TDSs	Total dissolved salts
$MgCl_2$	Magnesium Chloride
KCl	Potassium chloride
$CaCl_2$	Calcium chloride
KNO_3	Potassium nitrate
AGMD	Air-gap membrane distillation
SEM	Scanning electron microscopy
EDS	Energy- dispersive X-ray spectroscopy
IC	Ion chromatography
MP-AES	Microwave plasma atomic emission spectroscopy
Cl-	Chloride ion
NO^{-3}	Nitrate
K^+	Potassium ion
Na^+	Sodium ion

List of symbols

$L/m^2.hr$ (LMH)	Liters per square meter per hour
mg L^{-1}	Milligrams per liter concentration
kWh/ m^3	Kilowatt hours per cubic meter
kWh	Kilowatt hours
Mol/L	Moles per liter or molarity concentration
L/day	Liter per day
cm/s	Centimeter per second
m/s	Meter per second
^oC	Celsius degree
mOsm/kg	Osmolality unit
µm	Micrometer
Psi	Pressure unit

cm	Centimeter
cm^2	Square centimeter
J_w	Water flux
ΔV	Change of draw solution volume
Δt (h)	Time in hour
A_m	Effective area of the membrane
m^2	Square meter
J_s	Solute concentration
C_e	Salt concentration of the diluted draw solution
C_0	Initial concentration of salt in the cumulative permeate
g L^{-1}	Gram per liter
V_e	Final volume of the feed solution
V_o	Initial volume of the feed solution
mm	Millimeter
L	Length
W	Width
H	Height
L/min	Liter per minute
J	Distillate permeate
Δg	Weight change of the permeate flux
g/m^2	Gram per square meter, unit of density of the permeate flux
R	Rejection rate. and are the (mg/L) respectively
C_f	Feed permeate concentrations
C_p	Distillate permeate concentrations
P_f	Feed pressure
η	Pump efficiency
Q_p	Net permeate flow
QD-out	Flow of the draw solution outlet
QD-in	Flow of the draw solution inlet

Est	Total specific energy consumption
P_D	Pressure of the inlet draw solution
$Q_{f\text{-}in}$	Feed flow rate
P_f	Hydraulic pressures of feed solution
P_D	Hydraulic pressures of draw solution
MATLAB	Computing and visualization software
S/A_{sc}	Collector surface area
U’	Heat loss coefficient
Mc	Mass of collector
$C_{p,\,c}$	Collector heat capacity
B	Absorptivity coefficient
I_t	Solar radiation intensity
$T_{a,\,t}$	Ambient temperature
$T_{c,\,t}$	Collector temperature
h_c	Heat transfer coefficient of collector
L_c	Length of collector
m_f	Fluid flow rate
M_f	Mass of circulating fluid
$C_{p,\,f}$	Flow liquid heat capacity
$W/m^2\ ^oK$	Watts per square meter-Kelvin
Kg	Kilogram
J/Kg K	joule per kilogram per kelvin
W/m^2	Watts per square meter
^oK	Kelvin
m	Meter
Kg/s	Kilogram per second
ml/min	Milliliter per minute

$g\ m^{-2}\ h^{-1}$ (g MH)	Gram per square meter per hour
kV	Kilovolt
μA	Microampere

Highlights

1. A hybrid FO-solar powered MD system is proposed for brackish water desalination.
2. Regeneration of fertilizer draw solutions was conducted using an MD process capable of being driven by solar power.
3. The FO flow rate and the MD temperature are the major parameters for controlling the energy consumption.
4. A new theoretical model is developed to predict the power output of the solar collector.

1. Introduction

The rapid increase of water demands, and limited water sources has led desalination to become an essential technology for water production [1]. As water shortage is a universal risk in the next century [2], the development of a cost-effective and energy-wise desalination processes to draw pure water from saline sources, such as seawater or brackish water can resolve this problem. Membrane-based technology is a useful process to separate salt ions from saline water, therefore, recovering drinking water and increasing the water production. However, this process can be capital and energy-intensive due to the cost of water treatment and the distribution of clean water to the consumers [3]. These crucial issues have motivated scientists to investigate sustainable solutions for generating drinking water, energy, and required nutrients for agriculture. Water and energy are correlated to each other as the generation of drinking water consumes high energy while producing power needs a quite high volume of water [4].

The implementation of forward osmosis (FO) has been hampered by the lack of a suitable membrane, an ideal draw solution, and draw solution regeneration system with high efficiency. Firstly, the optimization of the support layer in terms of the structural parameter to reduce internal concentration polarization (ICP) is a significant challenge to the development of efficient FO membranes [5]. Furthermore, the research on the synthesis of the effective selective layer is hindered by the availability of materials for the interfacial polymerization process (IP). Intensive studies in the literature highlighted the modification of the selective layer to manufacture high perm-selective FO membranes and low fouling propensity [6]. However, most of

the attempts on membrane modifications to fabricate appropriate membranes for FO process have not been commercialized yet.

Secondly, a wide range of media as draw solutions have been reported in earlier studies and classified as traditional draw solution including gas or volatile compounds, organic solutes, inorganic solutes, polyelectrolyte draw solutes, novel draw solution such as stimuli-responsive polymers and nanoparticles, hydro-acid complexes, and functionalized nanoparticles [7, 8]. However, there are some critical drawbacks related to the draw solution separation, regeneration, and severe reverse solute flux. The later caused a reduction in the effective osmotic pressure and addition of more contaminants into the feed solution. When fertilizer draw solution was used for the FO system, the interaction of this draw solution with the membrane material may alter the structure of the membrane [9, 10]. Also, the final draw solution should be further diluted by potable water to obtain the required concentration for irrigation water.

More importantly, FO should be accompanied by a recovery system to regenerate the draw solution and extract potable water from the diluted draw solution. Essentially, the production of drinking water can be performed by a second recovery system such as RO [10], ultrafiltration (UF) [11], nanofiltration (NF) [12], membrane distillation (MD) or thermal processes [7]. However, these methods require high energy harvesting and capital cost to regenerate the diluted draw solution. For example, thermal-based desalination such as multistage flash (MSF, 21%), multiple-effect distillation (MED, 7%), and pressure-driven membrane desalination process including reverse osmosis (RO, 65%) are the most widespread desalination processes [13]. One of the limitations of thermal-based desalination system is high energy consumption exhibiting 10–16 kWh/m^3 for MSF and 5–9 kWh/m^3 for MED [14]. In case of RO system, electricity is predominant thereby the specific energy consumption (SEC) is lowered to 0.5–2.5 kWh/m^3 for brackish water reverse osmosis (BW RO) and 3–4 kWh/m^3 for seawater reverse osmosis (SWRO) [15]. Even though RO consumes lower energy, it is still cost and power-intensive process due to applying higher hydraulic than the osmotic pressure of the salty feed solution [1]. Several recent researches have reported that FO, MD, NF, electrodialysis (ED) and the use renewable power such as solar, geothermal, wind, wave, and ocean are alternative desalination processes with improved energy efficiency. FO can be an effective process for treating brackish water [7], digested sludge [16] and municipal wastewater [17]. Nevertheless, the energy cost of pumping the feed and draw solutions in the FO system might be a crucial factor in the operating expenditure. Several compartments responsible for the energy consumption in FO such as the pumps, draw solution regeneration, pretreatment of the feed solution and the draw solution and posttreatment of the brine, and fouling mitigation [18].

These limitations have sparked a renewed interest in exploring effective draw solution recovery system accompanied the FO desalination process. For example, Tan et al. [19] used hybrid FO-NF process for seawater desalination. The results revealed that the water flux approached 10.0 L/m^2. hr (LMH) for both methods and the salt rejection via the FO membrane was above 99.4 % for organic and inorganic draw solutions. The solute rejection by the NF membrane achieved 97.9 %, but the recovery of the draw solution required two cycles to produce drinking water. This resulted in high energy input and operating cost.

Similarly, Zhao et al. [12] used this recovery system with sodium sulfate (Na_2SO_4) or magnesium sulfate ($MgSO_4$) draw solutions for brackish water desalination. It was commented that the water flux decreased corresponded 8.0 LMH most probably due to membrane fouling. Therefore, it showed lower water flux reduction leading to high flux recovery after cleaning the membrane. The NF regeneration system exhibited fair salt rejection of 97.7% and the good quality of the product water. It was indicated that this hybrid system outperformed the RO alone process in terms of lower applied pressure, improved flux decline, higher flux recovery, no need for pretreatment step.

Renewable energy was used in desalination technology to reduce the energy input and overall cost of water production [20] as he pointed out that the energy consumption accounts for half of the capital costs of a desalination process. When photo voltaic-powered membrane filtration process (e.g., UF-RO/NF) was employed to filter brackish water with a concentration of 5300 mg L^{-1}, the specific energy consumption was estimated by 2.3 kWh/ m^3, water recovery of 28%, and the water permeate had acceptable quality. Zhang et al. [21] inspired by this process and proposed novel FO coupled solar-powered electrodialysis (ED) process for brackish water desalination. The aim was to minimize the power input and the cost of water productivity. It was found that a low simulated water flux of 3.5 LMH was obtainable when utilizing 1.0 mol/L NaCl as draw solution and brackish water feed in the FO system. After treating the diluted draw solution in the solar-powered ED, the energy consumption was decreased to 5.5 kWh/m^3 using 0.2 mol/L sodium chloride (NaCl) as a draw solution , the water product estimated by 130 L/day and had the same quality of the potable water. However, the capital cost involving purchasing membranes and solar panels was high of about 3.32 to 4.92 EUR m^{-3} per year for bench scale system. Besides, this system can be feasible to desalinate low salinity brackish water only.

Moreover, MD system operated by solar energy or waste heat or geothermal power can be used to recycle the draw solution and generate potable water. It involves a thermal separation process associated with membrane process in which the membrane is placed between cold and hot solutions. A result of the temperature difference across the hydrophobic microporous membrane, the water vapors transferred through the pores and condensed on a cold plate. A complete rejection of the solute can be achieved, leading to the production of drinking water [22]. Doung et al. [22] studied FO coupled direct contact membrane distillation (DCMD) system for seawater desalination. It was reported that when recycling brine into the feed tank, optimal water recovery from 20 to 60 % was achievable. This allowed a minimum specific energy consumption by half fold, and insignificant fouling was observable. At higher feed temperature to 50 ^oC, and a lower flow rate, the thermal efficiency of the DCMD system was improved remarkably. Besides, the warmer feed solution enhanced the transport of high salinity feed solution accomplishing high water recovery.

To achieve better performance the AGMD configuration including an air gap on the outlet side was used in this work. It was commented that air gap can minimize the heat lose by temperature polarization and maximizing the salt rejection [23].

This work aims to find the viability of using an FO coupled solar powered-MD system to desalinate brackish water and recycle fertilizer draw solutions. Firstly, the FO system was used as a treatment method and the performance of the modified FO membrane was investigated. Major operating factor (recirculation rate) affecting the FO energy consumption was optimized. Secondly, the efficiency of the MD recovery system in regenerating the diluted fertilizer draw solutions was also explored. Finally, the energy consumption of the MD system was estimated, and a new theoretical model was established to predict the thermal energy produced from a solar collector to minimize the energy consumption of the MD system.

2. Materials and methods

2.1 Membranes

Polyethersulfone (PES) UF membranes (UP150T) were purchased from Microdyn-Nadir GmbH, Germany which functioned as a support layer. The positively charged selective layer was fabricated on the top of the support layer based on the layer by layer procedure in our earlier research [24]. The optimal membranes modified with 2.5 bilayers including Sodium carboxymethyl cellulose (CMCNA) and Poly (diallyl dimethyl ammonium chloride) (PDADMAC) as a polycation polyelectrolyte and poly (sodium 4- styrenesulfonate) (PSS) as a polyanion polyelectrolyte were selected for the present work.

Th commercial membrane distillation (HVHP) made of Polyvinylidene Fluoride (PVDF) and has a sponge-like structure. The mean pore size is 0.45 μm, the average thickness is 115 μm, and the liquid entry pressure ($_{LEP}$) is ≥ 15 Psi as provided by the manufacturer.

2.2 Feed and draw solutions

In all FO filtration tests, deionized water (DI water) and synthetic brackish water solutions were utilized as feed solutions. The composition of the synthetic brackish water was described in our earlier work [10]. The synthetic brackish water was prepared with different total dissolved salts (TDSs) ranged from 10, 000 mg/L to 20,000 mg/L by adding NaCl, Magnesium Chloride ($MgCl_2$), Na_2SO_4, potassium chloride (KCl), and calcium chloride ($CaCl_2$) to DI water. A solution containing commercial fertilizers of KCl or KNO_3, or mixture KCl+KNO_3 were added to the DI water to prepare a draw solution with nutrients. Various concentrations (0.1, 1.5, and 0.2 mol/L) were used for all the draw solutions. NaCl aqueous solution was also utilized as a reference draw solution for comparison. All chemicals were acquired as a laboratory-grade from Merck, UK.

2.3 Fertilizer driven FO performance test

The bench scale FO system set-up was given in our previous work [10]. In brief, the system consists of a flat custom-made cell with dimensions of 16.6 cm × 8.6 cm, a total active area of membrane around 8.4 cm^2, two

reservoirs for the draw and feed solutions, and a data recording system. The draw and feed solutions were introduced to the membrane cell at a flow rate of 100 mL/min, which depicted a cross-flow velocity of 5.2 cm/s using two gear pumps. Two flow meters (Omega) were used to adjust the flow rate of both the draw and feed solutions. The initial volume of both the draw and feed solutions was fixed at 2.0 liters. The temperature of both the solutions was kept constant at 20.5 ^{o}C. The conductivity of the feed and draw solutions were measured through two conductivity meters (Jenway Man-Tech 4510, UK) and HI-8734 Multi-range TDS Meter (HANNA instruments, UK) during the experiments. The water flux over the membrane was determined based on the change of volume of the draw solution in time which was recorded with a computer-interfaced balance. All the experiments were performed with the active layer facing the feed solution configuration in counter current flow. After FO experiments, the diluted draw solution was transferred to the feed tank of the MD system for recycling.

The following formula was used to calculate the water flux.

$$J_w = \frac{\Delta V}{A_m \times \Delta t} \quad (1)$$

In which, J_w is the water flux (L/m^2. hr or LMH) and ΔV is the change of draw solution volume during an hour, Δt (h). A_m is defined as the effective area of the membrane, m^2.

The solute concentration in the feed solution (J_s) at any time was quantified as follows:

$$J_s = \frac{(C_e V_e) - (C_o V_o)}{A_m \Delta t} \quad (2)$$

Where C_e and C_0 are the salt concentration of the diluted draw solution and the initial concentration of salt in the cumulative permeate, g L^{-1}. Ve and Vo are the final volume of the feed solution, L and the initial volume of the feed solution which was 2.0 L respectively.

2.4 MD system

The current work utilizes a lab-scale air-gap membrane distillation (AGMD) system comprising a feed tank, a water-circulating gear pump, stainless steel cell, temperature sensors, a magnetic flow meter, and two pressure gauges as illustrated in Fig. (1). The feed tank can be filled up to 15.0 L solution. It has a heating element and the temperature was monitored by an Autotune temperature controller. A rectangular stainless-

steel cell placed horizontally to accommodate the membrane. It composed of three sections: feed chamber; air gap channel and cooling plate. The external size of the feed chamber is 145×95×55 mm length × width × height (L×W×H). The feed channel has a size of 520×4×3.2 mm (L×W×H) and the effective membrane area is 36.88 cm^2. The width of the air gas was approximately 8.5 mm. The size of the coolant plate 100 × 50× 15 mm (L×W×H) where the water vapour was condensed and flowed to the membrane cell at flow rate of 8.5 L per min (L/min). An aluminum spacer with size of 100 × 50 cm acted as a support for the membrane. The warm saline solution flowed across the evaporator channel at a fixed flow rate of 1.2 L/min using a gear pump (Tuthill Pump Co., UK). Water vapor passed through the membrane to the distillate channel, while the warm concentrate retentate was returned to the feed tank. The temperature of the warm feed and cold water was measured by thermocouples and the signals were transferred by a TC-08 thermocouple data logger (Pico technology) to the computer. The weight of the permeate distillate with time was measured by a digital balance (Precision Lab Balance) connected to data acquisition system. Eq. (3) and (4) were employed to calculate the distillate permeate and the salt rejection as follows [25]:

$$J\left(\frac{L}{m^2.h}\right) = \frac{\Delta g}{A.\ t.\ P} \tag{3}$$

Where, J is the distillate permeate, Δg depicts the weight gain of the permeate flux (g) over time (h). p denoted the density of the permeate flux (g/m^2). A is the effective membrane area (m^2).

$$\text{R (\%)} = \frac{C_f - C_p}{C_f} \times 100 \tag{4}$$

Where, R represents the rejection rate. C_f and C_p are the feed and the distillate permeate concentrations (mg/L) respectively. It should be mentioned that FO-MD system was employed for stand-alone FO and MD experiments.

2.5 Modeling energy consumption in FO system

The total energy consumption can be quantified as the sum of specific energy in both the feed and draw streams reservoir. Eq. (5) can be utilized to calculate the specific energy consumption, Es in the feed stream as follows [26]:

$$E_{sf} = \frac{P_f * Q_{f-in}}{36 * \eta * Q_p} \tag{5}$$

In which, P_f and η described the feed pressure and the pump efficiency. Q_p denoted the net permeate flow which is defined as the difference between the flow of the draw solution outlet ($Q_{D\text{-}out}$) and the draw solution inlet ($Q_{D\text{-}in}$). By Substituting Eq. (5), the Es in the draw solution stream of the FO membrane can be expressed as:

$$E_{sD} = \frac{P_D * Q_{D-in}}{36*\eta*(Q_{D-out}-Q_{D-in})} \quad (6)$$

Where, P_D denoted the pressure of the inlet draw solution. By combining eqs. (5) and (6), the total specific energy consumption (Est) in the FO membrane can be rephrased as:

$$E_{sD} = \frac{1}{36*\eta* Q_p} \quad (P_f Q_{f-in} - P_D Q_{D-in}) \quad (7)$$

$$E_{sf} = \frac{P_f * Q_{f-in}}{36*\eta*Q_p} \quad (8)$$

As the feed flow rate and the draw flow rate were equal ($Q_{f\text{-}in}$=$Q_{D\text{-}in}$) and the hydraulic pressures of both solutions were maintained constant (P_f = P_D), Eq. (8) can be rewritten as:

$$E_{st} = \frac{1}{36*\eta*Q_p} \ (2QP) \quad (9)$$

2.6 Solar collector

Water heating for MD can be performed using a solar collector. Modelling in the present work was based on a solar collector from SchücoSol K due to the availability of the information required for the theoretical modeling [27]. It was made of Aluminium Black and covered by a Sunselect absorber coating and a high−transparency glass on the top. Also, it had thermal insulation to prevent the loss of energy. The water can be circulated through the solar collector, which absorbs thermal energy from the collector and transfers it to a heat exchanger. It was assumed that there is insignificant heat loss from the solar collector as the water drawbacks do not evaporate under 100 ^oC. The collector angle was suggested 35^o during the summer to harness the maximum solar irradiation. While the collector tilt could be a number equal to the latitude plus ten degree [28]. This may empower the solar collector with the maximum solar radiation during the winter.

2.7 Development of a theoretical model for the solar collector

The practical electrical energy of the pumps was measured by digital meters connected to the rig. It should be noted that the solar collector was not used in the experiment, but theoretical calculations were performed to estimate the power out from the solar collector. A program was developed based on state-space model using MATLAB (The MathWorks Inc., version R2018b, US) to solve the energy balance equations. The state space model uses state variables x(t) to illustrate a system by several differential equations [29]. These variables can be rewritten from the theoretical input and output data to predict the power out from the solar collector. The variables with their values and units were described in Table.2. Inspired by [30] the governing energy balance equations for the solar collector including an absorbing metal plate and a heat fluid were modified as follows:

$$\frac{\mathrm{d}T_c}{\mathrm{d}t} = A_{11}T_c + A_{12}T_f + B_{11}Ir + B_{12}T_a \tag{10}$$

$$\frac{\mathrm{d}T_f}{\mathrm{d}t} = A_{21}T_c + A_{22}T_f + C_{21}T_{int} \tag{11}$$

Where T_{int} denotes the temperature of the fluid entering the collector through the pipes, which, for simplicity, has assumed equal to the external ambient temperature Ta. The coefficients are given by:

$$A_{11} = -\frac{S}{M_c C_{p,c}}(U_1 + h_c) \tag{12}$$

$$A_{12} = \frac{Sh_c}{M_c C_{p,c}} \tag{13}$$

$$B_{11} = \frac{SB}{M_c C_{p,c}} \tag{14}$$

$$B_{12} = \frac{SU_1}{M_c C_{p,c}} \tag{15}$$

$$A_{21} = \frac{Sh_c}{M_f C_{p,f}} \tag{16}$$

$$A_{22} = -\frac{1}{M_f}\left(\frac{Sh_c}{C_{p,f}} + m_{f,c}\right) \tag{17}$$

$$C_{21} = \frac{m_{f,c}}{M_f} \tag{18}$$

The form of each coefficient results from the derivation outlined in the Supplementary Information, wherein the energy balance of the system is considered. It should be noted that whilst the coefficients A_{11}, A_{12}, B_{11}, B_{12} and A_{21} are identical to those given in [29], A_{22} and C_{21} differ from the corresponding coefficients employed therein. These disparities result from the differing approaches used to model the rate of change of the total thermal energy of the fluid as a result of flow in and out of the system: whereas [30] described this variation using the partial derivative of T_f with respect to the distance travelled by flowing fluid through the collector, the present treatment instead makes the assumption that fluid present in the collector is at a uniform temperature, from which it follows that the energy difference between fluid entering and leaving the system is directly proportional to T_{int}-T_f.

Using the procedure given in the Supplementary Information, Equations 10 and 11 may be decoupled to produce the second order differential equation,

$$\frac{\mathrm{d}^2 T_c}{\mathrm{d}t^2} + a\frac{\mathrm{d}T_c}{\mathrm{d}t} + bT_c = g$$

where

$$a = -(A_{11} + A_{22})$$

$$b = A_{11}A_{22} - A_{12}A_{21}$$

$$g = B_{11}\left(\frac{\mathrm{d}Ir}{\mathrm{d}t} - A_{22}Ir\right) + B_{12}\left(\frac{\mathrm{d}T_a}{\mathrm{d}t} - A_{22}T_a\right) + A_{12}C_{21}T_{int}$$

Having decoupled the two starting equations, an analytic solution may be determined for T_c and subsequently T_f; using the values provided in Table 2, these solutions may be used to plot the two temperatures as a function of time.

The total energy transfer to the fluid, Q_f, is related to T_f and T_{int} via the specific heat capacity of the fluid, $C_{p,f}$, and the fluid mass flow rate, m_f. Information regarding this relationship is provided in the Supplementary Information, from which one obtains the expression,

$$Q_f = C_{p,f}m_{f,c}\int_0^t (T_f - T_{int})dt'$$

The variation of Q_f as a function of t can be determined.

2.8 Response surface modeling

Response surface modelling was used to optimize the most important process conditions for FO and MD systems. Firstly, the maximization and minimization linear formulas in Excel sheet were applied [31]. The formula was the energy consumption multiplied by the reverse solute flux or salt rejection and divided by the water flux. The multi-objective optimization was essential due to the importance of controlling the operating parameters for both systems to reduce the cost and commercialization. Thus, the optimization objectives in FO mode involved the water flux, reverse solute flux, and energy consumption. In MD mode, the optimization objectives included the permeate distillate, salt rejection, and energy consumption. This optimization procedure was used to obtain a balance between high water permeation, maximum production, and minimum energy consumption. Secondly, the range analysis values from the linear formulas were plotted in a response surface graph to distinguish the optimum value of each factor.

2.9 Designing a solar radiation profile for the Gulf region and Formulation models

It is also essential to describe the available solar radiation profile for the Gulf region. The solar radiation energy in Kuwait has been reported for 21 years [32]. The Gulf region had the greatest solar radiation in the summer and even in winter as the main reduction is in the ambient temperature while the sun shine is almost the same all year around. The peak of solar radiation average daily hour is 4.5 to 5.5 and estimated more than 950 W/m^2 at noon [32]. However, this value can be decreased to 500 W/m^2 at noon in the winter. Although this reduction, the energy generated can still be viable for the process operation. In this work, the solar radiation profile described the radiation generated during an average daily hour of 12.0 (from 6.0 am to 6.0 pm).

For the given solar radiation profile in Fig. (2), the analysis was carried out for a day, and the primary conditions were set at the intensity of 1042 W/m^2, the ambient temperature of 50 ^oK and time of 12 hours.

Next, the solar radiation profile described in the figure was acquired from the meteorological and solar energy reports, as mentioned previously.

The formulas used to predict the temperature have been given in equs. 10 and 11. It was followed by using the information of solar radiation and average temperature per 12 hours for the city. By using curve fitting in MATLAB, an eighth-order polynomial was obtained pertinent to the weather of the city, as shown in Fig.2:

3. Characterization and analytical methods

3.1 SEM

The surface and cross-section of the tested membranes were first coated by chromium with a thickness of 10 nm using a sputter coating instrument (Q150TS, Quorum Technologies, UK). The tested FO membranes were characterized by a Scanning electron microscopy (SEM) instrument coupled with energy- dispersive X-ray spectroscopy (EDS) (S-4800, Hitachi, Japan). The acceleration voltage and current were 2.0 kV and 5 μA respectively.

3.2 IC and MP-AES

Samples used were first diluted by adding 0.1 ml of the analyte to in 5 ml and 10 of DI water. The concentration of anions such as Cl-, NO^{-3} in the draw solutions were analyzed by ion chromatography (a Dionex ICS-90, UK). The concentration of ions can be determined based on the retention time and quantifies sample by integrating the peak area. Then, the of ions can be identified by comparing the peaks of the known standard solution to that of the analyzed concentration samples. Chromeleon software was used to tabulate the concentration of ionic components automatically. Moreover, 1.0 ml of analyte was diluted by 1.0 L DI water before MP-AES analysis. The cationic components such as K^+ and Na^+ were analyzed using Microwave Plasma Atomic Emission Spectroscopy (MP-AES, USA). By comparing the emission of a cationic component to that of known concentration of a component in a standard solution which was plotted in a calibration curve, the concentration of a component in analyte can be quantified.

4. Results and discussion

4.1 Performance of FO system using modified FO membrane

4.1.1 Water flux

The main purpose of using FO system is not only to produce diluted fertilizers for fertigation but also as a pretreatment stage to reduce the contents of total dissolved salts by many orders of magnitude. During the FO tests, draw solutions with several different concentrations of 1.0, 1.5, and 2.0 mol/L and different concentrations of synthetic brackish water (5,000- 10,000- 15,000- 20,000 mg/L) were utilized in the FO bench-scale unit. The water flux of the tested FO membrane was lowered as compared to the neat PES membrane due to tighter pores of the support layer and the presence of a dense selective layer, as shown in Fig. (3). The water flux as a function of the draw solution concentration, it was observed that the mixture draw solution produced comparable water flux and reverse solute flux to individual draw solutions. This can be ascribed to the highest osmotic pressure of the mixture draw solution than other draw solutions. The

osmotic pressure of the draw solutions is described in Table.1. Likely, there was an increase in the recovery rate upon increasing the concentration of the draw solution . The highest recovery rate was 53.3 %, achieved with 1.5 mol/L draw solution. In contrast, the water recovery rate was declined remarkably to 38%, obtained with the 2.0 mol/L draw solution. There was a linear correlation between the low concentration of the draw solution and the water flux for all the draw solutions. The same observation was reported by Achilli et al. [33] as a higher concentration of the draw solution was tested; the water flux was changed significantly. The water flux difference followed the order NaCl > KCl > KCl+KNO_3 > KNO_3 (see Fig.4) when using the same concentrations. This finding might be ascribed to the different osmotic pressure calculated by van't Hoff equation, which produced a large osmotic pressure value with a small molecular weight at a constant concentration [34]. At a concentration of 1.0 mol/L, the KCl and mixture KCl+KNO_3 scored the highest water flux of about 14.0 and 13.7 LMH which was slightly reduced to (13.5 and 13.3 LMH). Although the same concentration of draw solutions was used, the osmotic pressure was varied depending on the dissociation of species in the tested draw solution [35].

A further increase in the water flux was pronounced upon increasing the concentration from 1.0 to 2.0 mol/L. However, as the water moved fast through the FO membrane, the concentration of the brackish water feed and its osmotic pressure were slowly increased. Meanwhile, the osmotic pressure gradient and the driving force were diminished, leading to a reduction in the water flux across the FO membrane when using higher concentration of the mixture draw solution. It is worth noting that a slower decrease in the water flux was observed for the tested membrane as compared to Toray membrane in our previous work [10]. Besides, other draw solution exhibited similar trends as the ion concentration of the draw solution was increased, a much greater osmotic pressure was produced and thus high water permeation. The water flux generated from KCl and NaCl solutions was higher than the water flux generated from the mixture KCl+KNO_3 and single KNO_3 draw solutions. It is important to note that the osmotic pressure gradient between the draw solution having a higher concentration of 2.0, mol/L (e.g., KCl+KNO_3 and KCl) and the feed solution was reduced faster thereby a more severe decrease in the water flux was observable. Increasing the concentration of all the draw solutions to 2.0 mol/L demonstrated a sharp decrease in the water flux due to the combined effects of ICP, fouling, composition, and concentration of the feed solution (see Fig.4-C). Even though the solution-diffusion principle indicates a linear correlation between water flux and draw solution concentration, FDFO filtration tests demonstrated a nonlinear relationship over the period of the test [36]. According to Stone et al. [37], the altered physicochemical characteristics of the draw solutions can also impact the membrane performance. For example, this can be raised from the dominant effect of an increase in the density in the mixture draw solution, including many components with different physical properties. Even though precipitation of salts on the selective layer contributed to a lower water flux, the severe reduction in the water flux was mainly caused by the diminished driving force and ICP effects [38]. To a certain extent, the thick support layer can act as a further resistance which obstructed the solute mass transfer aiding to a higher ICP and lower water permeation. Based on the simulation data, it was found that the maximum recovery rate was approached 53.5 % and was reduced due to the dilution of the draw solution by pure water from the feed solution.

Figure. (4) presents the water flux as a function of the feed solution concentration instead of the draw solution concentration and compared between different draw solutions. Interestingly, there was not a linear increase in the water permeation upon increasing the concentration of the draw solution. Another group of researchers as exemplified by Wang et al. [39], a similar trend was highlighted when using brackish water and seawater as the feed solutions. The water flux began decreasing more sharply upon increasing the concentration of the feed solution. This suggested that both the osmotic force and water permeability were changed at the same time. Likely, the dramatic reduction in the water flux was again accompanied by a change in the feed solution properties as the scale precursors exceeded their solubilities and precipitated out of the feed solution forming a scaling layer. As expected, the NaCl draw solution caused a no noticeable fouling while the brackish water feed showed considerable scaling. This scaling fouling on the selective layer blocked the transport of water molecules, thereby further decrease in the water permeation was noticeable.

4.1.2 Reverse solute flux

A higher reverse solute flux always occurred when there was higher water permeation across the membrane. Initially, the NaCl and KCl draw solution had the highest reverse solute flux around 33.3 and 31.2 g MH because of low molecular weight and small hydration radius of ions [39]. However, the mixture KCl + KNO_3 achieved the lowest reverse solute flux in the range of 20.4 – 6.3 $g.m^{-2}$ h^{-1} (g MH) when using various draw solution concentration (1.0-1.5-2.0 mol/L) and different feed solution concentration (5,000-10,000-15,000-20,000 mg/L).

As anticipated, the specific salt flux should be recorded to determine the quantity of draw solution loss during the FO desalination. The specific salt flux defined as the ratio of reverse solute diffusion to the water permeate (J_S/J_W) per unit of water permeate [40]. The trend of specific salt flux was in good agreement with the results of reverse solute flux, which is in accordance with Yang's study [34]. Therefore, great osmotic pressure and high concentration of the draw solution will favor the reverse solute diffusion flux. Likely, when draw solution with higher molar concentration, the J_S/J_W became greater. For instance, the highest J_S/J_W was obtained with single KNO_3 draw solution ranging from 0.66 to 1.52 under the same conditions. The even lower J_S/J_W was produced by single KCl draw solution corresponding 0.45 and increased when using higher molar concentration. A drastic fall in the reverse solute flux was observed at longer operating time, and this trend was also noted when using a higher concentration of the brackish water feed as previously addressed in the literature [36]. Generally, the permeability−selectivity trade-off implied an increase in the water flux, followed by an increase in the solute flux [41]. On contrary to this, the results indicated that the performance of the tested membrane did not exhibit the same concept. In case of using mixture KCl+KNO_3draw solution , the reverse salt flux intended to decrease as the water flux was greater as shown in Fig.5. Among the three draw solutions at the same molar concentration of 1.0-1.5-2.0, the KCl + KNO_3 draw solution turned out as the best performing draw solution for the FO process by generating a minimum specific salt flux of 0.44 followed by KCl draw solution which was recorded as 0.45 (see Fig.5). This means that the loss of the

$KCl+KNO_3$ draw solution to the feed solution was negligible and it remained nutrient-rich solution. Based on these results, it is clear that the minimum cost of regeneration can be assigned for the $KCl + KNO_3$ draw solution as compared to others. Besides, the examined membrane can offer better advantages such as good selectivity and favorable dense active layer thickness.

Regarding ionic rejection, the highest rejection was achieved for K^+ ions as the concentration of the in the KCl and mixture $KCl+KNO_3$ draw solutions remained high, e.g. 1.5 and 2.0 mol/L. However, traces of K^+ ions were detected of about 520 and 730 mg/L in the feed solution when using concentrated KCl and $KCl+KNO_3$ draw solutions respectively. On the other hand, NO_3 ions could pass easily through the membrane due to the rapid reverse solute flux from the draw solution to the feed solution upon increasing the draw solution concentration, and they were accumulated in the feed solution. The concentration of the NO_3^- ions in the feed solution was measured as high as of about 932 and 780 mg/L in the KNO_3 and $KCl+KNO_3$ draw solutions respectively. It was found that the tested KNO_3^- draw solution exhibited much different K^+ and NO_3^- rejection of the examined FO membrane. It may be explained by a strong electrostatic repulsion occurred between the K^+ and the positively charged amine group in the selective layer leading to a greater rejection rate of K^+. In the same time, the electrostatic attraction between NO_3^- and positively charged surface facilitated the passage of these ions to the feed solution, thereby lower rejection rate.

On the other hand, there was a weak repulsion force established between the negatively charged NO_3^- and the selective layer. This may cause adsorption of these ions on the surface and hence, poor rejection rate. Additionally, high ionic concentration of monovalent ions such as Na^+ and Cl^- was measured in the feed solution due to the reverse salt flux. It is worth mentioning that the Cl^- ions were hardly diffused through the selective layer as its hydrated ionic radius is greater than that of Na^+ ions [41]. These investigations clearly indicated that the ionic rejection rate was proportional to the concentration of the draw solutions. This can be attributed to the increase in the driving force, which was augmented by increasing the molar concentration of the draw solution. Furthermore, retentions of the salt ions tend to increase, and the flow of the solute from the draw solution was slowed down with a higher concentration of the synthetic brackish water feed. An explanation can be found in the possible change of the surface morphology, thicker scaling layer, porosity, pore size, and selectivity of the active layer. It should be mentioned that the concentration of these nutrients was exceeded the acceptable limit of nutrients in standard irrigation water and thus further dilution for the final draw solution is required. The FO membrane in the present work showed little improvements as the reverse salt flux was slightly enhanced without a sharp drop in the water permeation as compared to Toray membrane.

4.1.3 FO membrane scaling

The morphology and microstructure of the FO membranes are provided in Fig. (6). It can be seen in Fig.5-A that the surface of the selective layer appeared to have crystalline scaling. It is most probably due to the exposure to high concentration of brackish water feed during the filtration experiments. A similar observation was indicated in earlier study by Mi et al. [42]. It was reported that the crystalline structure depicted calcium sulfate dihydrate scaling. The scaling layer was formed on the selective layer due to the presence of scaling precursor such as calcium and sulfate in the brackish water feed. In comparison with our previous work when using Toray membrane, the tested membrane showed thinner and a much loose structure with smaller crystals of scaling on the selective layer. This might be attributed to the positively charged selective layer which caused strong repulsion between the charges of the modified selective layer and salt ions. This indicated that the positively charged selective layer slightly minimized the growth of salt crystals and less affected by scaling layer. In addition, this may indicate that the material and modification procedure of selective layer material significantly inhibited the formation of scaling layer. Since the structure of scale created on the modified selective layer is less compacted, it can be suggested that the chemistry and positive charges of the selective layer can reduce crystallizing than negatively charged PA selective layer of Toray membrane. Moreover, Fig. (6-B) showed no significant change on the structure of the support layer after filtration tests. The images demonstrated that the porous support layer free of pore clogging which implied that the fouling occurred mainly on the selective layer. This explained that the scaling layer on the selective layer hampered the reverse diffusion of retained solutes into the support layer aiding to rapid flow of water through the membrane, better water permeation and reverse salt flux.

4.1.4 Estimating the energy expenditure under controlled circulation rate

The flow rate of the draw solution plays a crucial role in the energy consumption of the FO process. The KCl + KNO_3 with 1.5 molar concentration and brackish water as a feed solution was selected to be applied in recirculation velocity tests. In this work, the electrical energy of the circulation pumps was measured by digital meters as described in Fig.7. The specific energy consumption of the pumps to recirculate the feed solution and draw solution was calculated as kilowatt-hour of electrical energy per cubic meter of the water permeate for 12 hours. It is generally agreed that a greater concentration of the draw solution resulted in high recovery rate, thereby relatively lower energy consumption. It was observed that when higher draw solution concentration of 2.0 mol/L was operated at constant circulation rate in the FO experiment, the water permeate was dropped remarkably around 9.1 LMH while the energy consumption remained constant. This decrease in the water flux might be related to the reduction in the water permeate and severe dilution of the draw solution during the same operating time. It was found that the maximum recovery rate was 53% when using 1.5 mol/L draw solution. As shown in Fig. (7-C), the results revealed an opposite trend when raising the

circulation velocity from (100 ml/min- 5 m/s to 150 mil/min-8 m/s), the energy consumed became higher (1.8 kWh).

To examine the effect of the circulation velocity, 1.5 mol/L KCl+KNO_3 draw solution was utilized and three flow rates/crossflow velocities of 50 ml/min- 5 m/s, 100 ml/min-8 m/s and 150 ml/min – 11 m/s were selected to obtain water flux from synthetic brackish water (5,000-10,000-15,000-20,000 mg/L). It was found that the water permeate was increased at a higher recirculation rate of 150 ml/min-11 m/s, as illustrated in Fig. (7-C). This can be ascribed to the decrease in the external concentration polarization upon increasing the flow rate of the KCl draw solution [43]. This is in accordance with Zou and Hu [43], as the energy consumption would increase from 0.02 to 11.93 kWh/m^3 owing to the higher flow rate from 10 to 250 ml/min. Since the greatest energy expenditure of this FO process was 0.97 kWh/m^3 at 150 ml/min-11 m/s, it was much lower than that for RO system for seawater desalination achieving 1.2–1.5 kWh/m^3 [44]. The energy demand was influenced significantly by higher recirculation velocity and increased by 60 % as compared to that with recirculation velocity of 50 ml/min-5 m/s. In comparison with the literature, the energy consumption of the present FO system at a flow rate of 50 ml/min was slightly higher of about 0.32 kWh/m^3 to that for FO process to treat seawater at a recovery rate of 50% (~ 0.11 kWh/m^3 at 50% recovery) [45]. A higher flow rate of the draw solution caused high energy demand, and the greatest specific energy expenditure was 0.97 kWh/m^3 under process conditions of 150 ml/min and 2.0 mol/L DS. Fig. (8) demonstrated that the optimum recirculation rate and electrical energy consumption were 50 ml/min and 1.2 kWh respectively. At this optimum recirculation rate, the optimal water flux and reverse solute flux were recorded as 8.1 LMH and 12.8 g MH respectively. It is realized that the minimum specific energy consumption was estimated by 0.32 kWh/m^3. Although this value was acquired for various draw solution, it could be reported as an approximate value for the system. In this respect, the total electricity consumption per cubic meter of water desalinated is substantially lower than other desalination systems mentioned previously. On the other side, if the energy required to regenerate the draw solution is considered, therefore the hybrid FO-MD process would consume higher energy than FO stand-alone system.

4.2 Water permeate and re-generation efficiency of the MD system

Following the FO desalination, the MD tests were performed using a lab-scale MD set up. These tests were conducted with feed solutions having a salt concentration of 0.8 to 1.4 mol/L NaCl and KCl solutions, 0.5 to 1.0 mol/L KNO_3 solution, and 0.16 to 0.3 mol/L KCl+KNO_3 solutions. Fig. (9) demonstrates the distillate production of different feed solution types and concentrations. The analysis data described an inverse correlation between the permeate flux with increasing feed salinity. It was revealed that the highest water flux was achieved when low concentration feed solution was used as a feed. The best performing feed solutions were in the order of NaCl > KCl > KNO_3 > KCl+KNO_3. It was found that the water flux generated

from low salinity feed solutions was far better than that obtained from those with higher salinity. Fig. (9) showed that the water flux was dropped by (30%) in distillate production when higher salt concentration was used as feed. For example, the water flux was reduced from 7.7 to 4.9 LMH when the concentration of KCl as feed solution was increased from 0.8 to 1.4 mol/L. Similar trends were observed for other feed solutions as higher salinity feed caused a serious reduction in the water flux. This is because of the well-known fact that the salinity affected the water vapor pressure of the feed solution with respect to the vapor pressure of the pure water and this decrease was severe at high feed temperature [46]. It is because the system is operated by heat transfer, and the high feed salinity caused a greater reduction in the temperature through the membrane. Thus, the high loss in conduction heat and low heat input for water evaporation resulted in minimum permeate distillate. Unexpectedly, these feed solutions (KNO_3 and $KCl+KNO_3$) having minimum salinity concentration associated with the lowest permeate distillate and the highest rejection rate. It was determined that the permeate flux.

In contrast, in parallel with increasing feed concentrations as 6.4 to 4.0 LMH and 6.0 to 3.8 LMH for KNO_3 with 0.5 – 1.0 mol/L and $KCl+KNO_3$ with 0.16 to 0.3 mol/L respectively. Besides, it was clear that the permeate distillate had lower salt concentration under the same operating conditions. This can be explained by other likable effects of the mass transfer of salt ions through the membrane and the solution composition. Based on this consideration, not only the feed salinity had a major influence on the permeate flux but also the composition of the inlet used in the system.

Additionally, the MD was super-efficient in the regeneration of the inlet since the solution was highly concentrated instantaneously through the MD system after it became diluted in the FO process. The quality of permeate distillate was assessed by means of conductivity measurements. The results showed the distillate had high purity as drinking water when lower concentration feed solutions. The average salt rejection was maximum achieving > 99.4 % when working with feed concentration between 0.1- 0.8 mol/L. Likely, the permeate distillate showed good purity when increasing the feed concentration to 1.44 mol/L. A small deterioration in the salt rejection was detected corresponding 98.5 %, but it was improved remarkably over longer operation time. However, prolonged running time might be influenced by the quality of the permeate distillate. The same finding was reported in the literature [47]. This is because the membrane became dry after many hours at high feed temperature resulting in the formation of salt crystals, thereby pore-clogging. Thus, a severe water flux reduction could occur during the experiments exacerbating the quality of the permeate distillate. It can be postulated that there was negligible difference in the conductivity measurements in all the permeate distillates indicating almost complete rejection of salt ions. It is worth quoting that the conductivity value of all distillates was always lower than the threshold level of 500 μS/cm satisfying the standard of drinking water. In conclusion, the process efficiency is less affected by the salinity concentration and concentration polarization as it was the case for the FO process. This proofed the effectiveness in the removal of salt components from water and recycling the diluted draw solution, demonstrating its feasibility in salt removal under the optimal conditions.

4.3 MD membrane fouling

Both inorganic fouling and wetting are critical elements hindering the performance of the MD process for desalinating saline solutions [48]. In this work, the inorganic salt interacted either with each other or with the membrane surface creating salt deposits. Fig. (10) showed a non-uniform distribution of a thick fouling layer on the top surface after 12 hours of inorganic salt solution exposure. It was observed that the fouling layer became thicker with increasing the time of exposure to the salt solution. It was found that a considerable build-up of the salt accumulated near the spacer and some salts were deposited in the pores. The results revealed that the permeate distillate was dropped sharply when increasing the salt concentration in the feed solution (see Fig.9). It can be ascribed to a fouling layer formed on the membrane surface or pores might be partially or completely blocked, decreasing the effective area for the vapor-liquid interface. These salt crystals filled the membrane pores decreased the porosity of the membrane, and it could be prone to membrane wetting. Another major effect is less hydrophobicity that was governed by the growth of salt crystals within the pores. It can be assumed that the porosity of the tested membrane was lowered significantly due to salt crystallization in the large pores. This is because the salt components can be transported easier in the big pores leading to the accumulation of salt crystals. According to Laqbaqbi et al. [49], these negative impacts can influence the wettability of the membrane over a long operating time. Thus, the transport of the solution can be limited through the fouling layer, causing a severe mass transfer resistance for the water.

It should be noted that salt components were trapped in the pores and wetting of the membrane was occurred. It was proven that the inorganic salt precipitation not only caused a sharp reduction in the water flux but also influenced salt rejection. Similar fouling behavior was also reported for MD membrane subjected to saline feed solution [50]. It can be expected that the performance of the tested membrane was also altered by temperature and mass polarization. As a result, a gradual decay in the water permeate could be aggravated by the high heat resistance of the fouling layer. It was found that the membrane behaved differently against feed solutions with various concentrations and composition. For example, upon increasing the temperature during the test, some of the salt became less soluble in the water which exacerbated the formation of salt crystals in the solution rather than on the membrane surface giving that the temperature was lower across the membrane surface. It can be suggested that the temperature polarization can be accelerated over time because the temperature on the permeate flux side became higher than that on the feed stream. In stark contrast, when the feed solution composed of highly miscible NaCl salt when increasing the feed temperature, the concentration and temperature polarization led to thick salt precipitation on the membrane surface. As mentioned above, the rejection rate for all the feed solutions was exceeded by 99.0%. We, therefore, conclude the membrane-less affected by the wetting when exposed to concentrated feed solution. It is possible to mitigate fouling by controlling the feed temperature and operating conditions in the MD system. Overall, the

FO pretreatment minimized the suspended salt concentration in the diluted feed solution, thereby an acceptable permeate flux, and high rejection was achievable.

4.4 Determining energy expenditure under controlled temperature

The effect of the temperature on the inlet diluted draw solutions with different concentrations (NaCl, KCl, KNO_3, and KCl+KNO_3) on the permeate distillate was investigated. The concentration and temperature of the inlet solution were varied of 0.3 to 1.6 mol/L and 40, 50, 60, 70 ^oC, respectively. The flow rate was fixed at 1.2 L/min, and the coolant temperature was constant at 7.1 ^oC. It can be seen in Fig. (11) that the increment of permeate distillate was linear upon raising the feed temperature or membrane trans-temperature difference. This led to an increase in the volume of pure water transporting from the inlet to the output water. The initial permeate flux was relatively persistent as the partial vapor pressure of liquid was little influenced by TDS concentration in the feed solutions.

The ranking of the inlet solutions in terms of highest permeate flux was in the order of NaCl > KCl > KNO_3 > KCl+KNO_3. This is because the water activity of these feed solutions was varied as the NaCl and KCl solutions had the greatest permeate flux at temperature ranged from 40 to 70 ^oC. It was stated that the water activity correlated to the feed concentration [51]. In fact, increasing the feed concentration leaded to low water activity thereby diminishing the effective water vapor pressure. This low water vapor pressure can influence the energy consumption remarkably. It can be suggested that a higher ratio between the vapor of the salt solute and the vapor of the pure water was higher for NaCl and KCl feed solutions as compared to other feed solutions. The permeate flux change was in good agreement with an earlier researcher [52] as the water activity of these feed solutions was a crucial element enhancing the permeate flux. Furthermore, the same figure indicated that at the highest temperature of 70 ^oC, the NaCl and KCl with a concentration of 0.86 and 0.82 mol/L achieved the highest permeate flux of about 9.4 and 8.5 LMH as compared to higher feed concentrations of 1.3 and 1.44 mol/L. This can be attributed to the improvement of thermal efficiency and driving force for the solution mass transport over time [53]. However, the mixture KCl+KNO_3 and KNO_3 with a concentration of 0.52 and 0.17 mol/L exhibited slightly greater permeate flux recorded as 6.7 and 5.8 LMH than that for feed concentrations of 1.0 and 0.3 mol/L. Similarly, the MD system achieved maximum salt rejection of 99.76 % feed solutions having lower molar concentrations while it was slightly reduced to 98.57% for feed solutions with higher molar concentrations.

On the other hand, increasing the salt concentration in the inlet solution influenced the permeate flux significantly. The reduction in the water flux is proportional to the TDS concentration in the feed solutions. It was observed that the permeate flux was dropped slightly when increasing the concentration of all the inlet solutions. The results revealed that higher TDS concentration of about 0.86-1.0 and 0.28-0.3 mol/L for KNO_3 and KCl+KNO_3 feed solutions respectively caused much lower permeate flux as compared to other feed

solutions at the same TDS concentrations. Besides, a rapid reduction in the permeate flux at a lower temperature of 40 and 50 ^{o}C was probably raised from lower water vapor pressure when using higher TDS concentration in the inlet solution. Therefore, the driving force for mass transport was minimized at higher TDS concentration of the inlet solution. According to Boubakri et al. [54], the permeate flux and driving force can be reduced at higher salt concentration due to concentration polarization (CP) effects on the membrane. At a temperature of 60 ^{o}C, there was less variation in the permeate flux between all the feed solutions while it was insignificant at 70 ^{o}C. The major reason for the improvement in the permeate flux was the solubility factor. The good solubility of all the salty feed solutions with different TDS concentrations caused higher permeate flux at higher feed temperature. The trends depicted in Fig. (11) were consistent with theoretical expectation [55]. It was stated that the solubility of salt solutions was enhanced when increasing the temperature yielding excellent permeate fluxes. Overall, the MD system was able to produce acceptable permeate fluxes, and it was enhanced drastically at higher feed temperature. The greatest permeate flux was produced at the highest temperature of 70 ^{o}C than that at lower temperatures. Figure. (12) revealed that the optimum permeate distillate was 5.7 LMH and salt rejection of 99.55 % at an optimum temperature of 60 ^{o}C. Taking into account the cost of energy consumption, operating the system with a high temperature of 70 ^{o}C could raise the heat energy consumption per unit of potable water to be generated, thereby increasing the water production cost. The city can be benefited from very high solar energy and access to brackish water.

4.5 Efficiency of the solar collector

The performance of the solar collector is expressed according to the energy output and energy consumed in the MD unit for water desalination. It can be seen that the energy output fluctuated as solar irradiation fluctuated. During the day, the highest temperature was between 06:00 am and 06:00 pm, which generated the greatest power output from the solar collector to the solution. As shown in Fig.2 the temperature and radiation rate changes during the day. It is shown that the feed solution at 70 ^{o}C can be produced throughout the day after 12 hours. During this period, the solar radiation rates reached a peak, and the temperature can be maintained at the maximum in the system. When the solar radiation rates and air temperature decreased, the heat exchanger with counterflow can boost the heat in the water flowing on the collector and the cold feed solution. Then, the cold feed solution in the feed tank can be transported into the heat exchanger to be warmed up and returned to the feed tank. It should be noted that there was an insignificant heat loss from the solar collector as it was assumed that the water does not evaporate at temperatures under 100 ^{o}C. It is recognized that the system utilized around 80% of the total energy output to desalinate the feed solution. The quantity of heat calculated to be provided by the solar collector is shown in Fig. (13). The total daily thermal energy that can be liberated from the solar collector and transferred to the solution was calculated to be 300 kWh. This amount of thermal energy is more than sufficient to operate the heater, which was recorded as 4.63 kWh/m^{3}. Even though the solar energy fluctuates due to changes in the time and weather, the energy generated from the solar collector is enough to heat the feed solution sufficiently to produce an acceptable

amount of permeate distillate with minimum conductivity. Excess energy can also potentially be converted to an electrical energy to operate the pump or the cooler and hence making the MD unit self -sustainable.. Thus, the total energy consumption of the MD unit (7.06 kWh/m^3) can potentially be minimized at as little as 1.1 kWh/m^3 if the cooler is fed from the solar energy, or theoretically to zero if both the cooler and the pump are operated by the solar collector. It is worth noting that the amount of solar energy generated during day time, can be also stored in batteries to operate the system on 24 hours' bases. This indicates that the total energy consumption of the hybrid FO-MD is much better than that for the RO technology for brackish water desalination.

5. Conclusions

In this work, the fertilizer driven FO coupled solar powered MD system was operated to produce irrigation water for fertigation, to regenerate the diluted draw solution, and to extract potable water. The performance of the hybrid FO-MD was analyzed. The solar collector was suggested to reduce the energy consumption of the MD system and the energy consumption was calculated simultaneously using advanced theoretical model. The highlights of this research are as follows:

1- For all the individual draw solutions, the FO system was able to generate high water permeation and acceptable reverse solute flux. However, the mixture KCl+KNO_3 achieved the lowest water flux and reverse solute flux. The maximum water recovery was reached 53.5% when using concentrated fertilizer draw solution and brackish water feed.
2- The FO membrane showed thin scaling layer on the surface depending on the concentration of the brackish water feed. It can be cleaned easily by circulated water at high flow rate in the system.
3- The optimum specific energy consumption of about 0.32 kWh/m^3 was accomplished at the lowest recirculation rate of 50 ml/min.
4- After the FO pretreatment step, the MD was efficient in producing drinking water achieving optimum water permeate of about 5.7 LMH and superior salt rejection of 99.55 % at an optimum temperature of 60 ^oC.
5- The MD membrane exhibited less fouling and insignificant wetting when using concentrated feed solution.
6- From our theoretical study of the combined solar collector-MD the energy consumption can be decreased from 7.06KWh/m^3 to 1.1 KWh/m^3 using solar heating and power.

Acknowledgments

The authors are grateful to Qatar National Research Fund, Qatar Foundation for Education, Science and Community Development for providing the PhD scholarship to W. Suwaileh. The authors wish to thank Dr. Mokarram Hossain from Zienkiewicz Centre for Computational Engineering, Swansea University for his help in mathematical calculations.

Figure Captions:

Figure.1: A schematic illustration of AGMD lab scale unit. (1) Chiller, (2) Feed tank, (3) Gear pump, (4) Flowmeter, (5) Membrane cell, (6) Electronic balance, (7) Thermocouple data logger, (8) Heater, (9) Heater controller, (10) Pump controller, (11) Thermocouple, (12) Pressure gauge, (13) Computer.
Fig.2: Average daily solar radiation profile of Kuwait City. The highest radiation occurs at temperature of 50 ^{o}C.
Fig. 3: Comparison between the water fluxes of the pristine and modified membranes.

Fig.4: (a) Water flux generated from NaCl, KCl, KNO_3, and KCl+KNO_3 draw solution with 1 mol/L against brackish water feed with concentration ranged from 5000 to 20, 000 mg/L. (b) Water flux generated from NaCl, KCl, KNO_3, and KCl+KNO_3 draw solution with 1.5 mol/L against brackish water feed with concentration ranged from 5000 to 20, 000 mg/L. (c) Water flux generated from NaCl, KCl, KNO_3, and KCl+KNO_3 draw solution with 2.0 mol/L against brackish water feed with concentration ranged from 5000 to 20, 000 mg/L.
Fig.5 : (a) Solute flux diffusion difference between reference NaCl, KCl, KNO_3, and KCl+KNO_3 draw solutions with molar concentration of 1.0 versus brackish water feed with concentration from 5000 to 20, 000 mg/L. (b) Solute flux diffusion difference between reference NaCl, KCl, KNO_3, and KCl+KNO_3 draw solutions with increasing the molar concentration 1.5 mol/L versus brackish water feed with concentration from 5000 to 20, 000 mg/L. (c) Solute flux diffusion difference between reference NaCl, KCl, KNO_3, and KCl+KNO_3 draw solutions with increasing the molar concentration 2.0 mol/L versus brackish water feed with concentration from 5000 to 20, 000 mg/L.

Fig.6: (a) the structure of salt crystals on a scaled membrane surface after FO desalination test using brackish water feed and concentrated mixture KCl+KNO_3 draw solution.

Fig.7: (a), (b) Energy consumption recorded for the feed solution and draw solution pumps over period of time of 12 hours respectively. (c) Impact of recirculation velocity on the energy consumption of the FO system.

Fig.8: Surface analysis identifying the optimal water flux, reverse salt flux and energy consumption values in the FO system.
Fig.9: Change in the cumulative distillate flux as function of feed solution concentration between 0.3 and 1.4 mol/L in the MD system.
Fig.10: Fouling on the membrane surface during the MD experiments using salty feed solution with concentration of 1.4 mol/L.
Fig.11: Permeate distillate variations with respect to the feed temperature ranged from 40 to 70 ^{o}C. MD. Tests were conducted with a constant flow rate of 1.2 L/min and coolant temperature of 7.1 ^{o}C.
Fig.12: Surface analysis showing the optimal water flux and energy consumption values in the MD system.
Figure.13: illustrating (a) ambient temperature during the day (^{o}K). (b) Temperature of solar collector during the day (^{o}K). (c) Initial fluid temperature (^{o}K). (d) Black line describes fluid temperature (^{o}K) and dotted line depicts initial fluid temperature (^{o}K). (e) Energy transferred to the solar collector (kWh). (f) Power output of the solar collector (kW).

Figures:

Graphical abstract

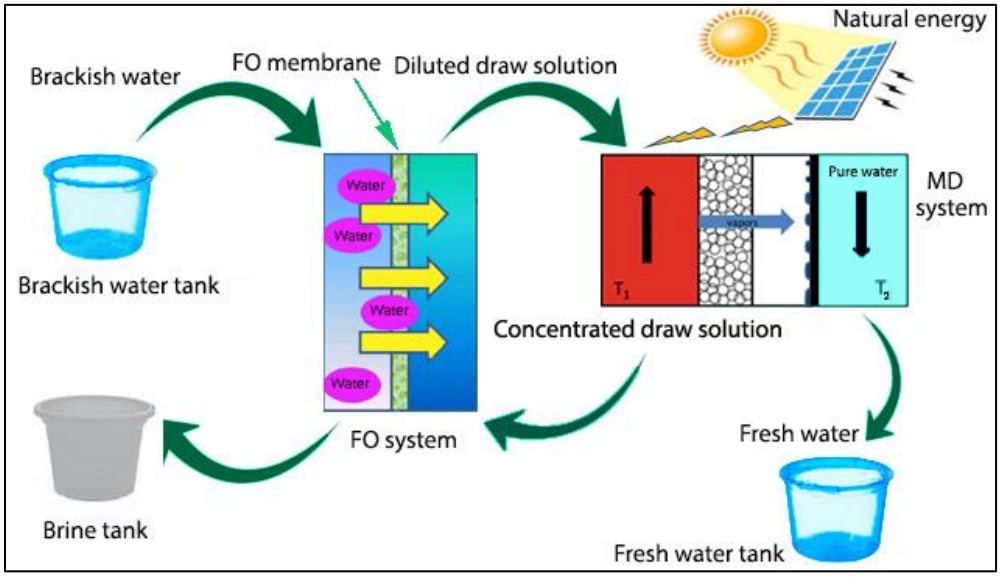

Fig.1

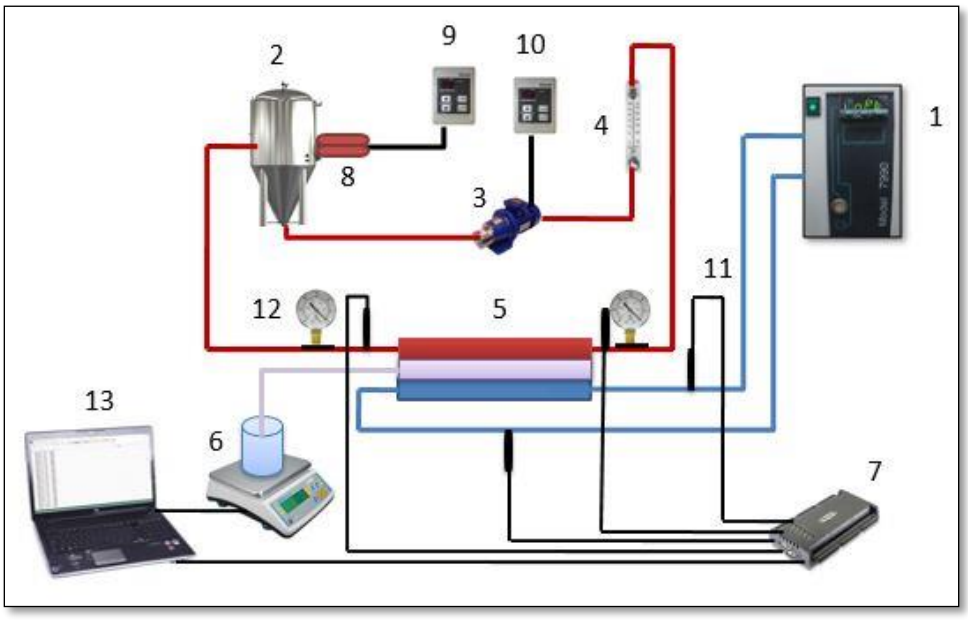

Figure.2

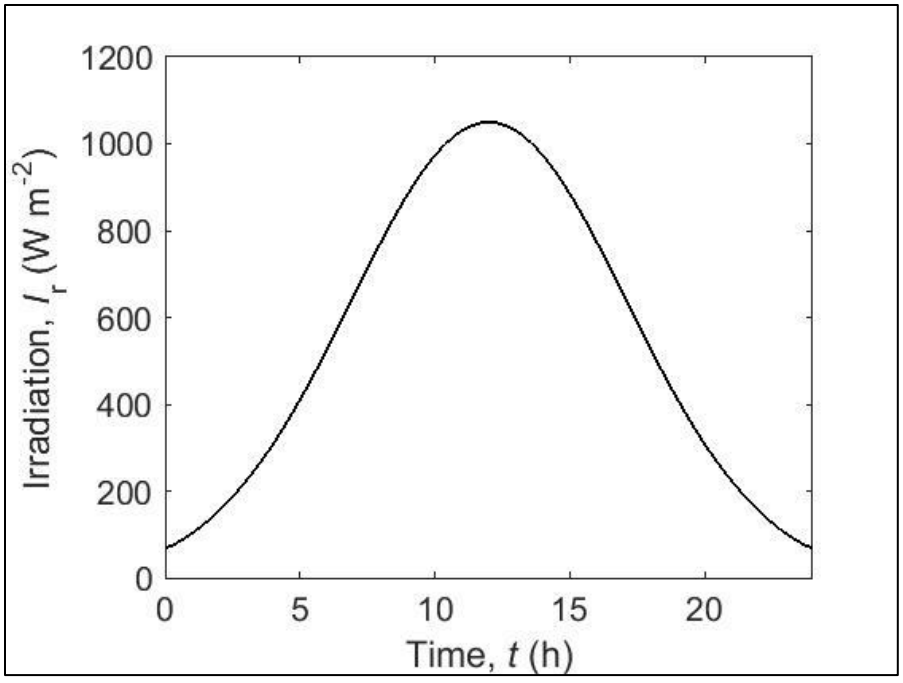

Figure.3

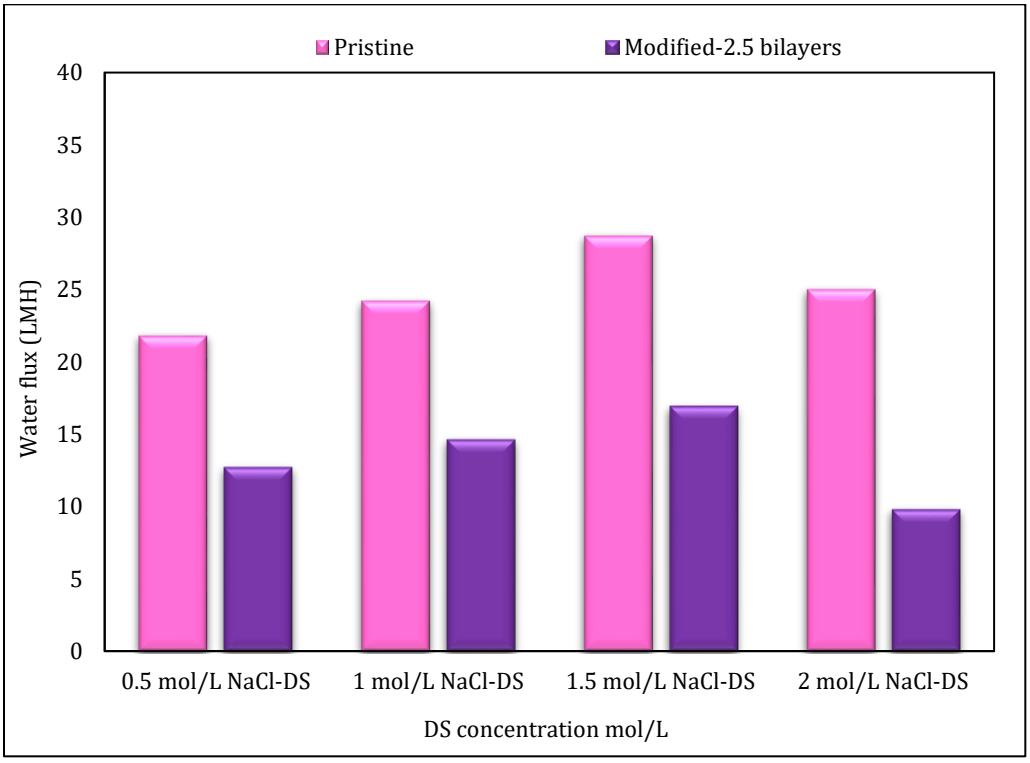
Pristine
Modified-2.5 bilayers
40
35
30
25
20
15
10
5
0
Water flux (LMH)
0.5 mol/L NaCl-DS
1 mol/L NaCl-DS
1.5 mol/L NaCl-DS
2 mol/L NaCl-DS
DS concentration mol/L

Figure.4

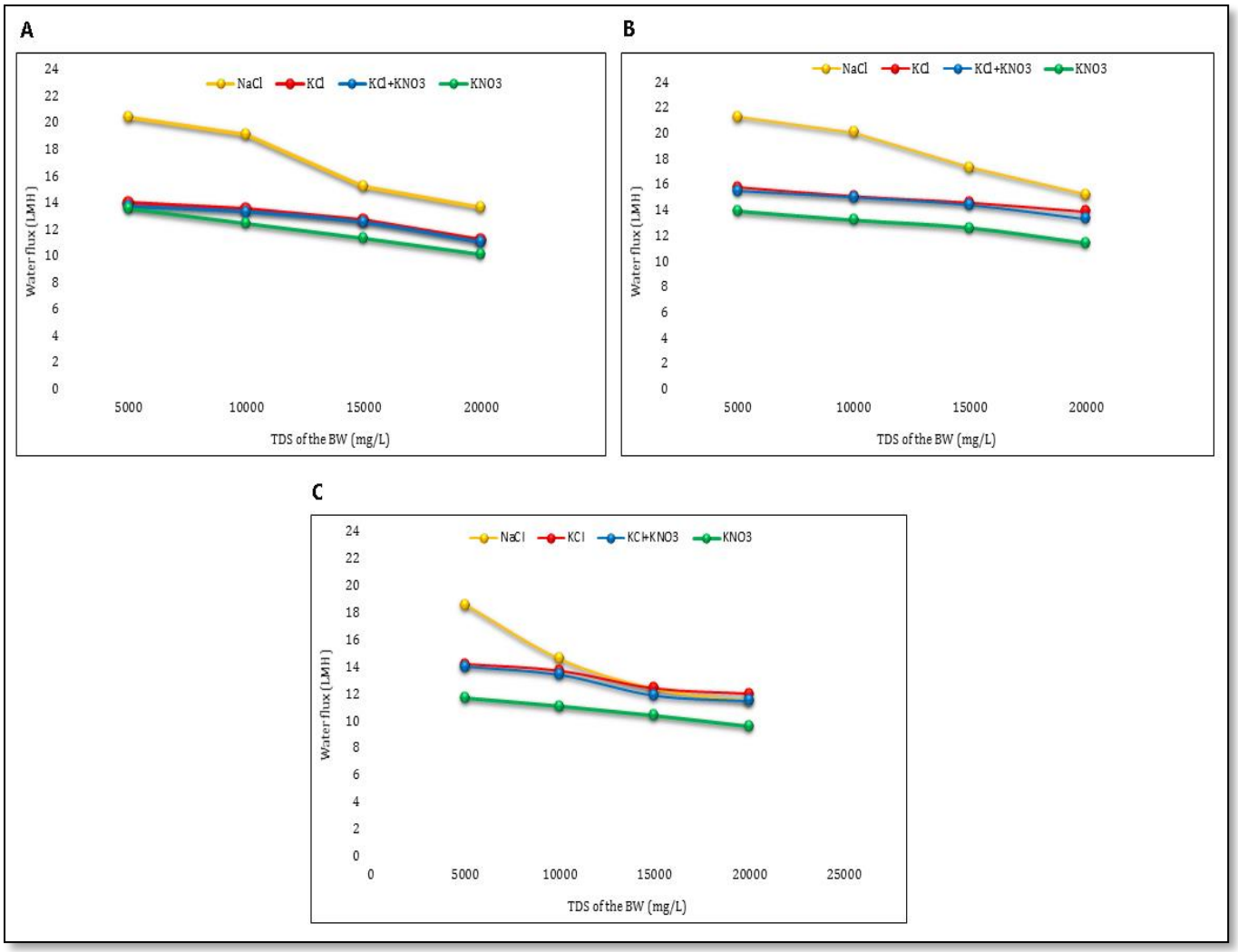
A
NaCl
Kcl
Kcl+KNO3
KNO3
Water flux (LMH)
TDS of the BW (mg/L)
B
NaCl
Kcl
Kcl+KNO3
KNO3
Water flux (LMH)
TDS of the BW (mg/L)
C
NaCl
KCl
KCl+KNO3
KNO3
Water flux (LMH)
TDS of the BW (mg/L)

Figure.5

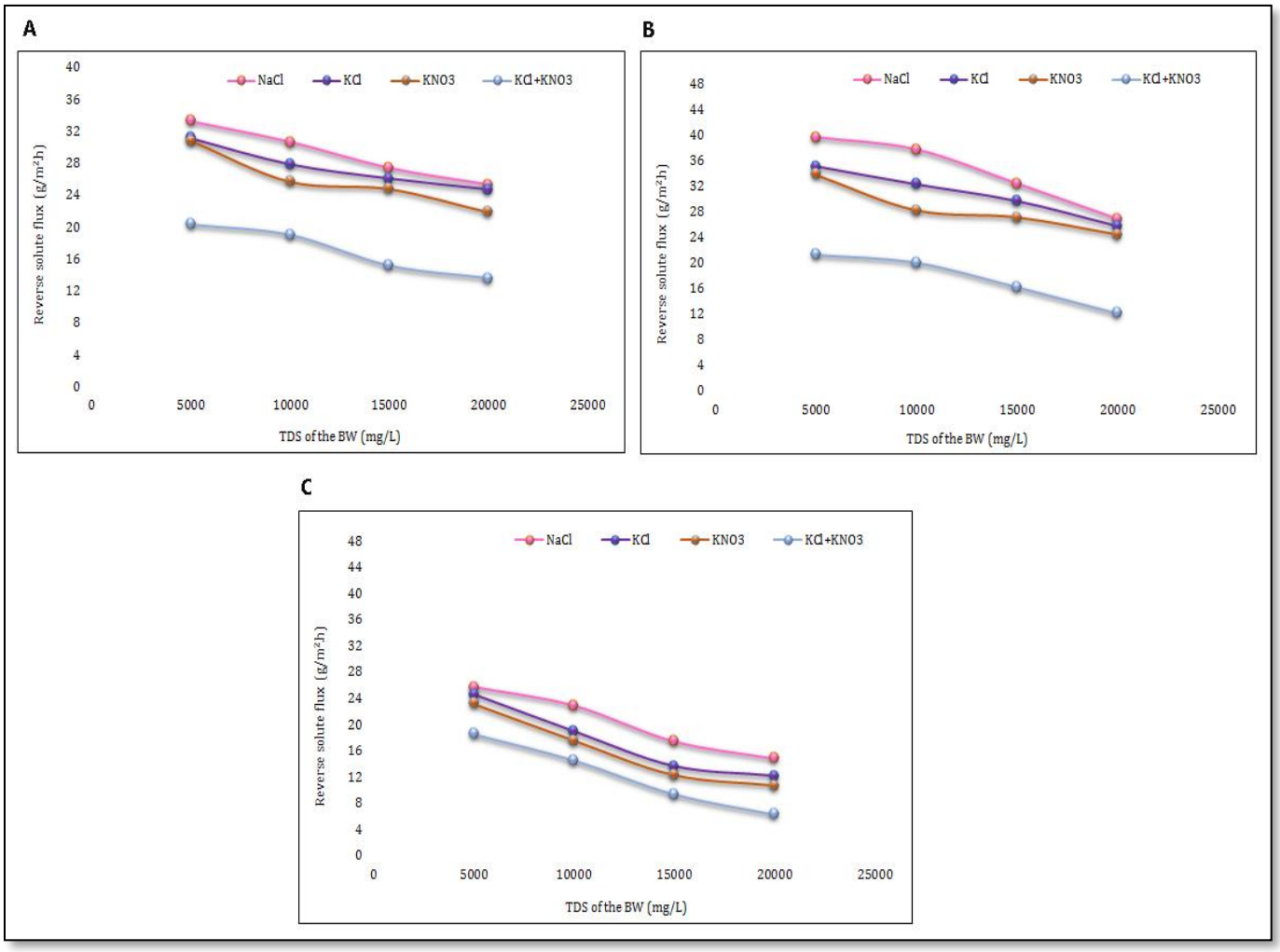
A
NaCl
Kcl
KNO3
Kcl+KNO3
Reverse solute flux (g/m²h)
TDS of the BW (mg/L)
B
NaCl
Kcl
KNO3
Kcl+KNO3
Reverse solute flux (g/m²h)
TDS of the BW (mg/L)
C
NaCl
Kcl
KNO3
Kcl+KNO3
Reverse solute flux (g/m²h)
TDS of the BW (mg/L)

Figure.6

A **B**

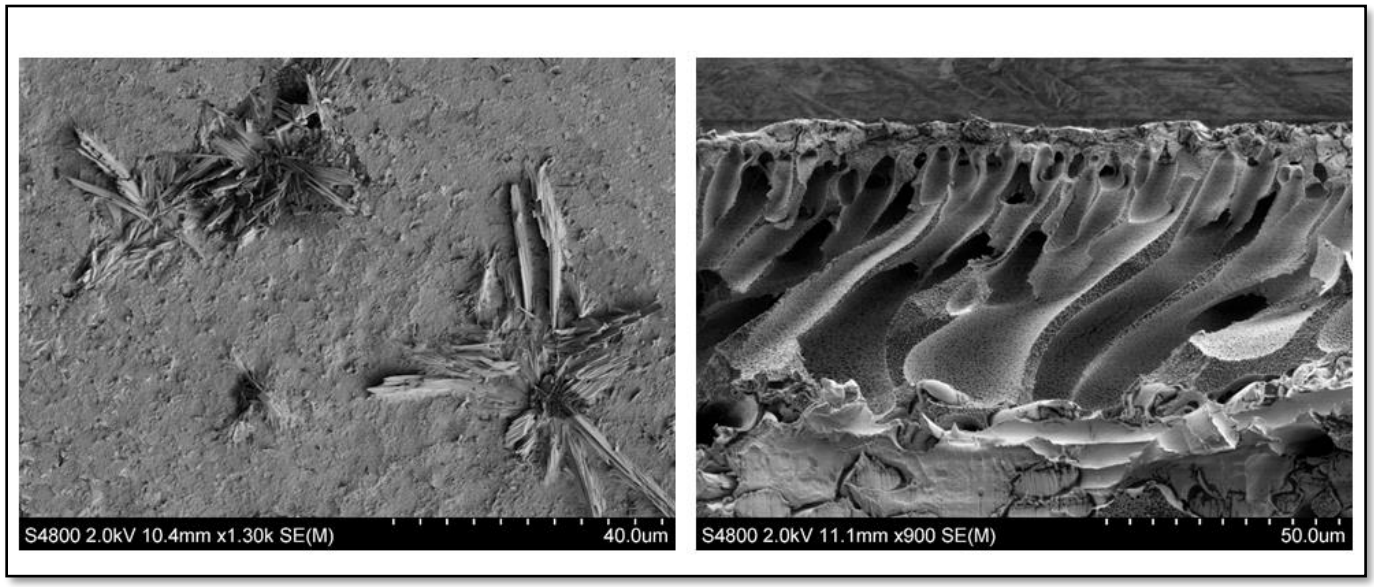
S4800 2.0kV 10.4mm x1.30k SE(M)
40.0um
S4800 2.0kV 11.1mm x900 SE(M)
50.0um

Figure.7

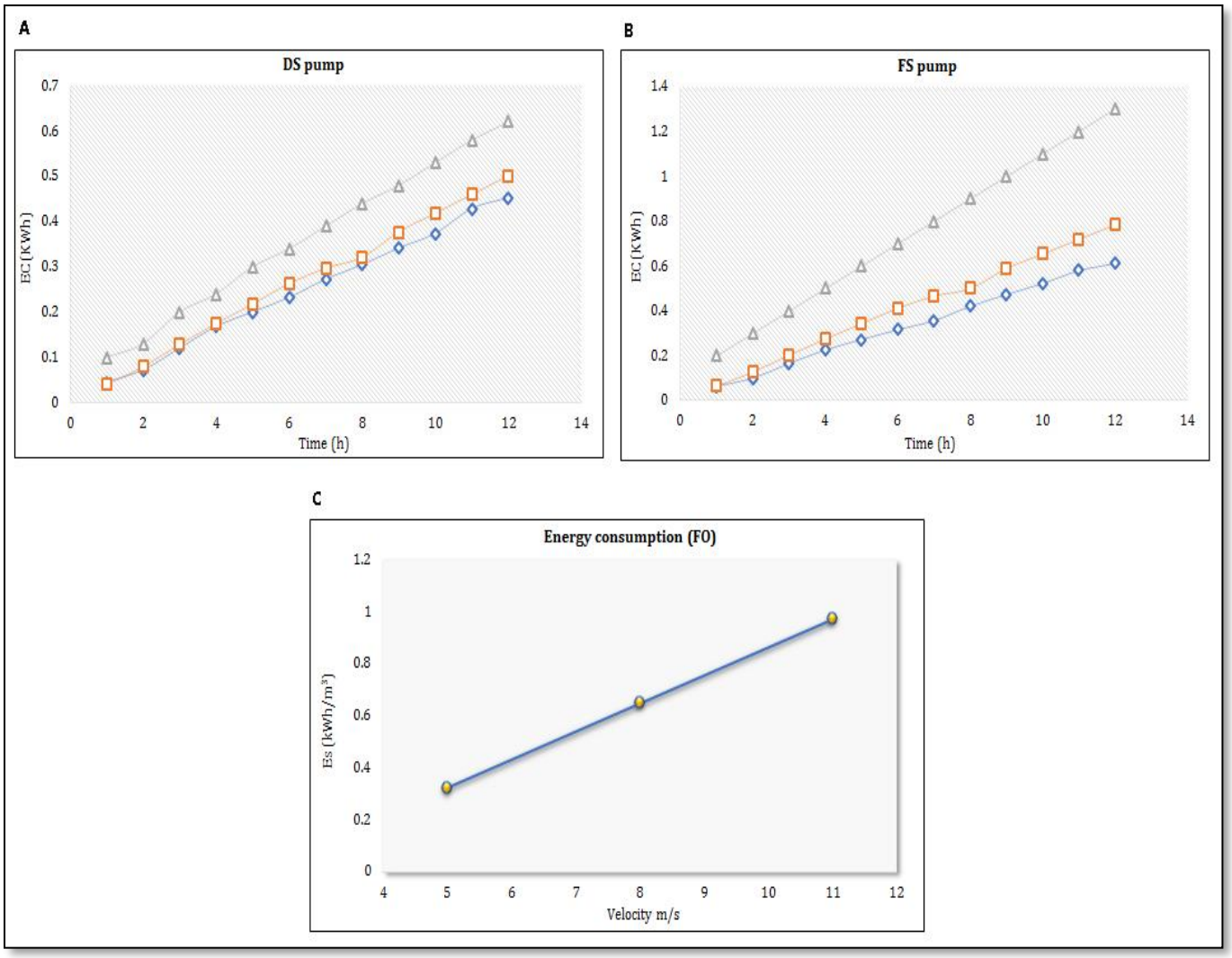
A
DS pump
EC (KWh)
Time (h)
B
FS pump
EC (KWh)
Time (h)
C
Energy consumption (FO)
Es (kWh/m³)
Velocity m/s

Figure.8

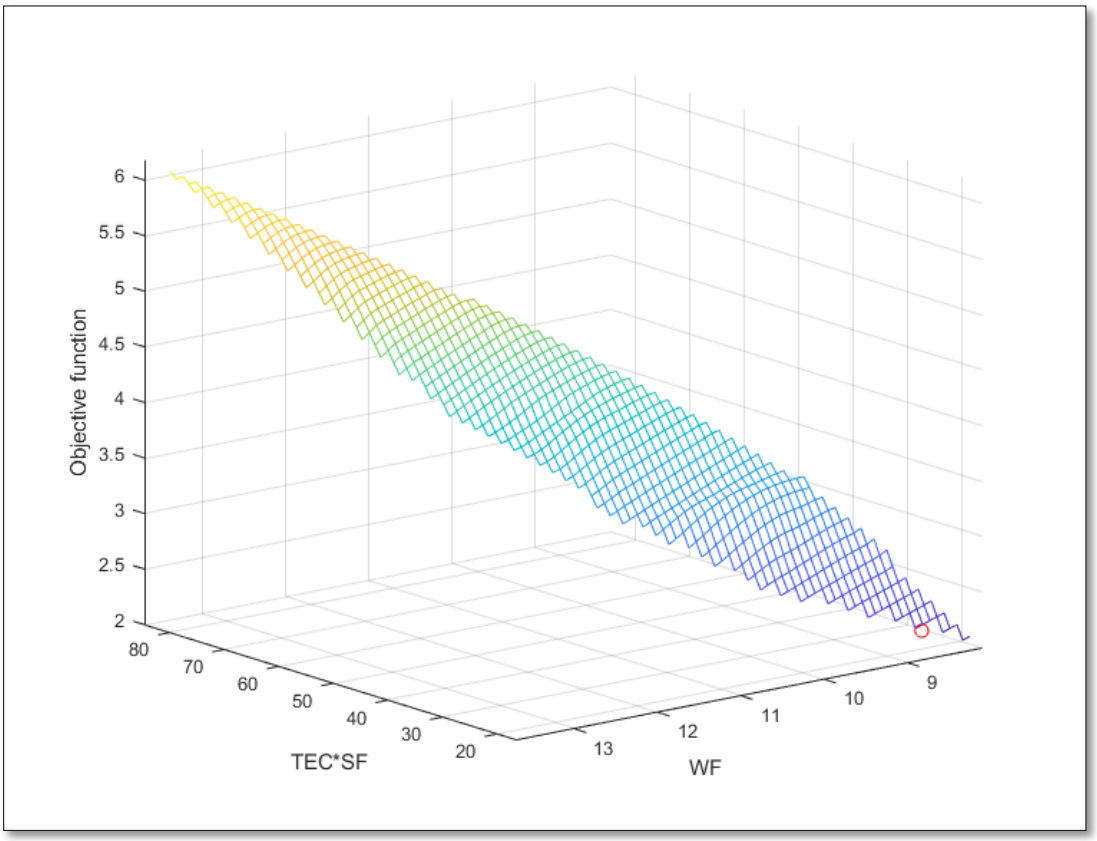
Objective function
6
5.5
5
4.5
4
3.5
3
2.5
2
80
70
60
50
40
30
20
TEC*SF
13
12
11
10
9
WF

Figure.9

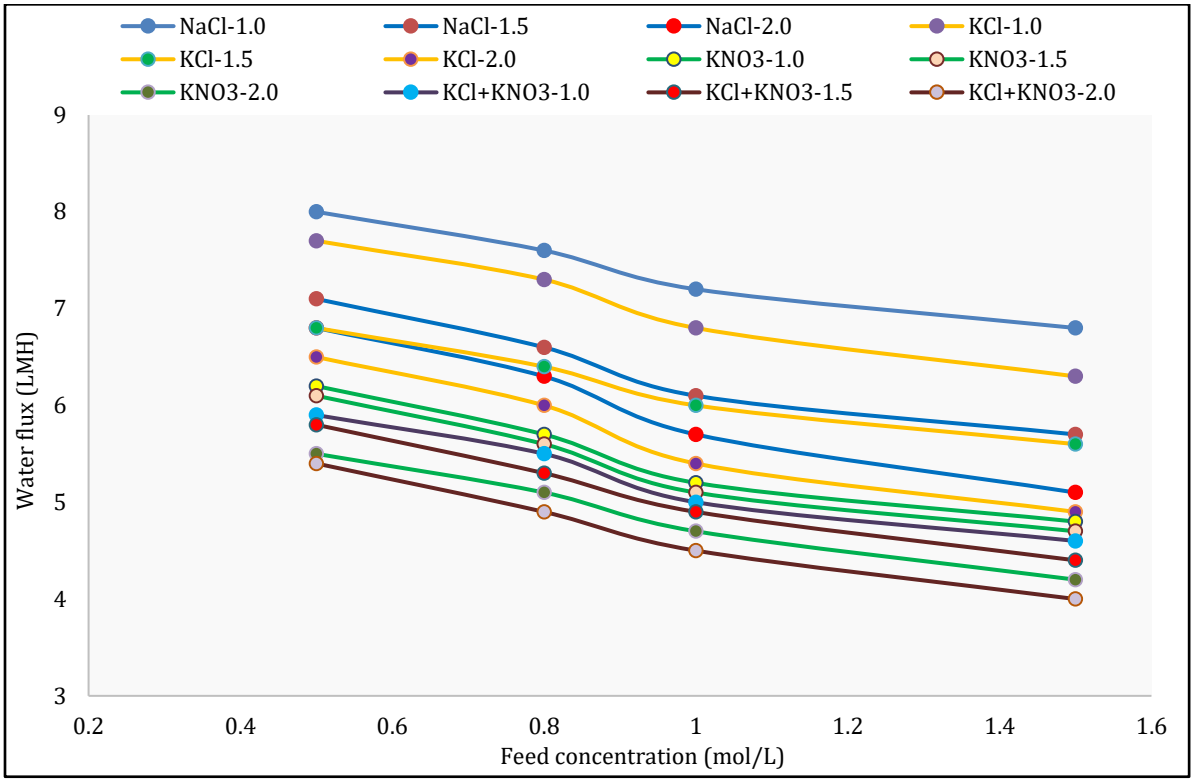

Figure.10

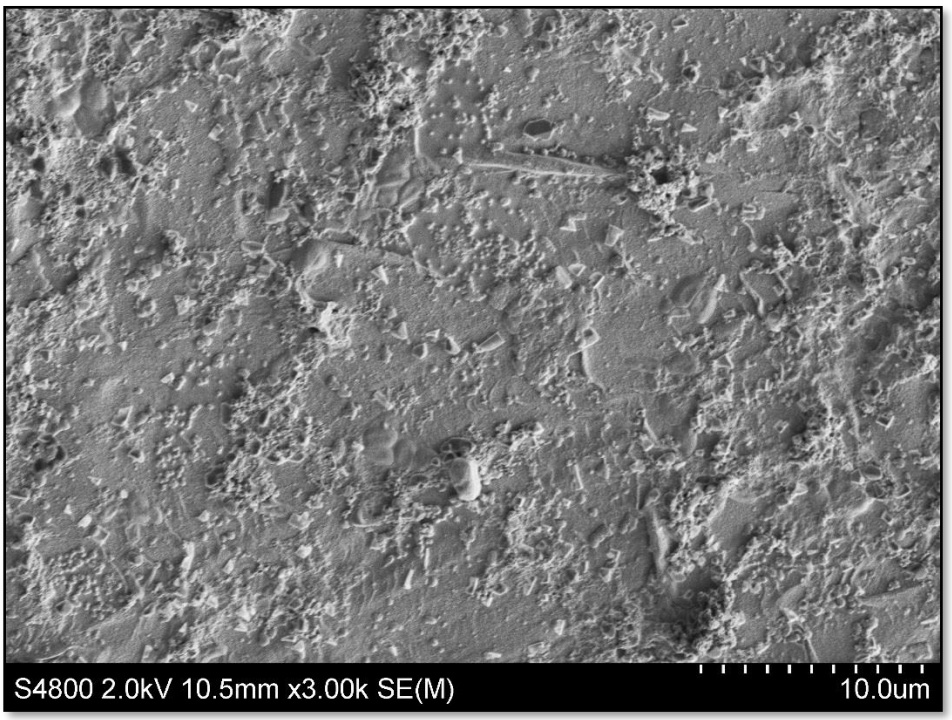

Figure.11

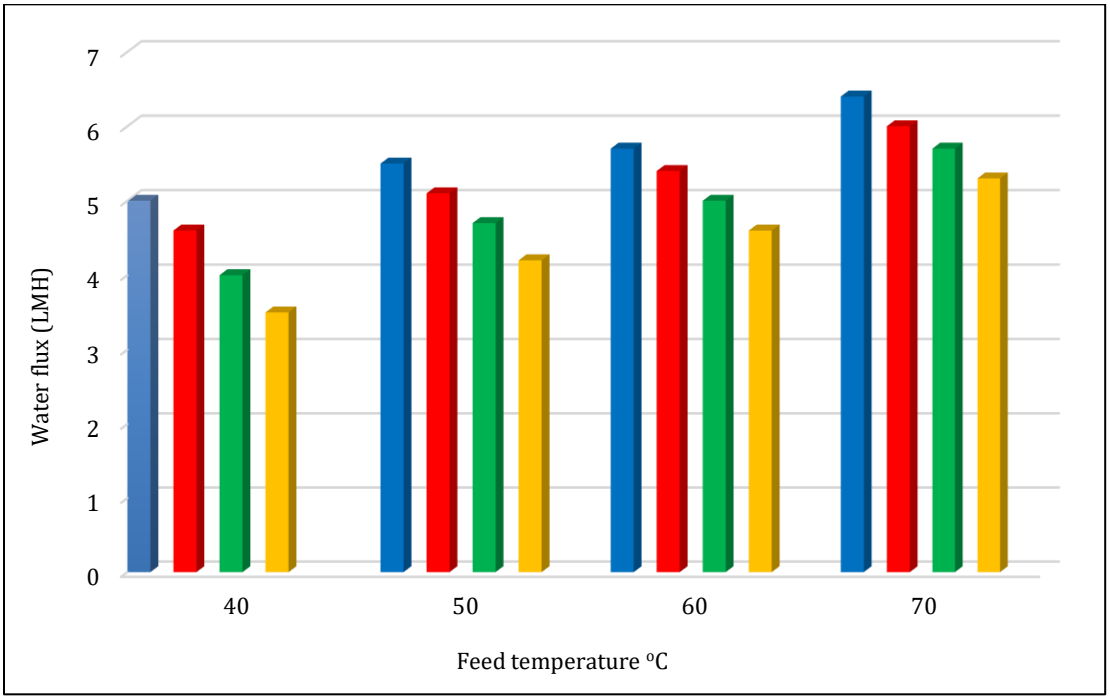

Figure.12

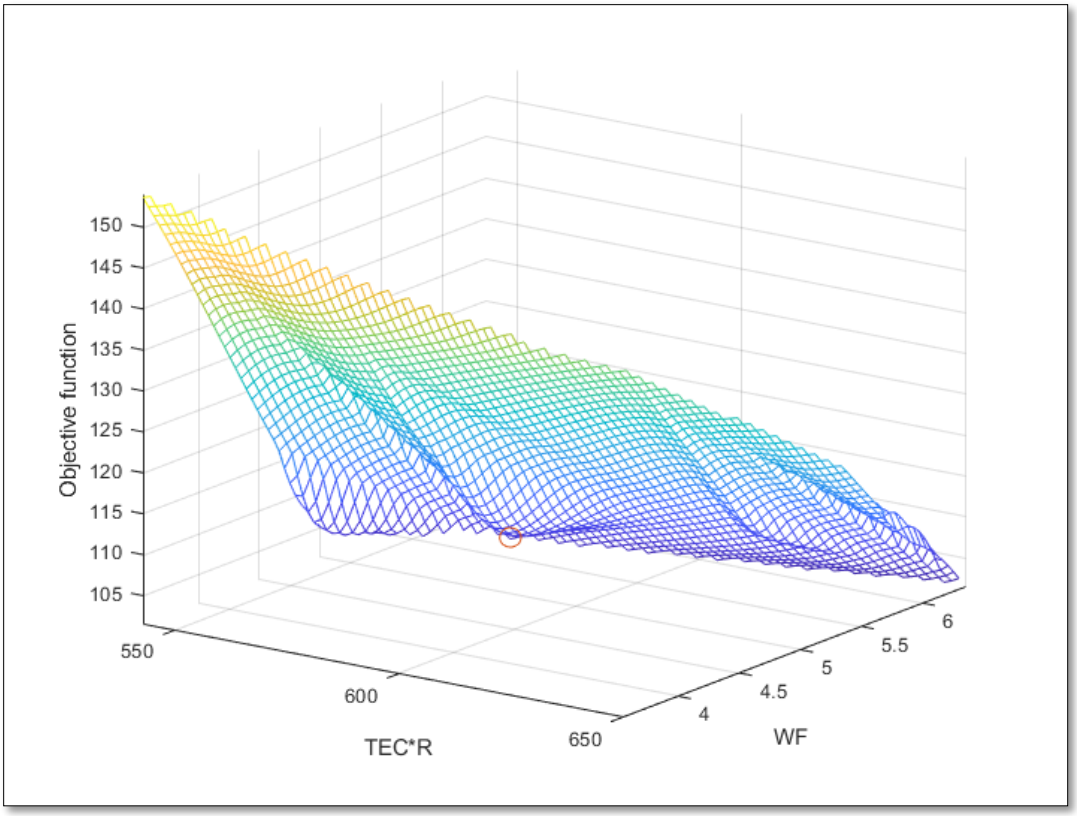

Figure.13

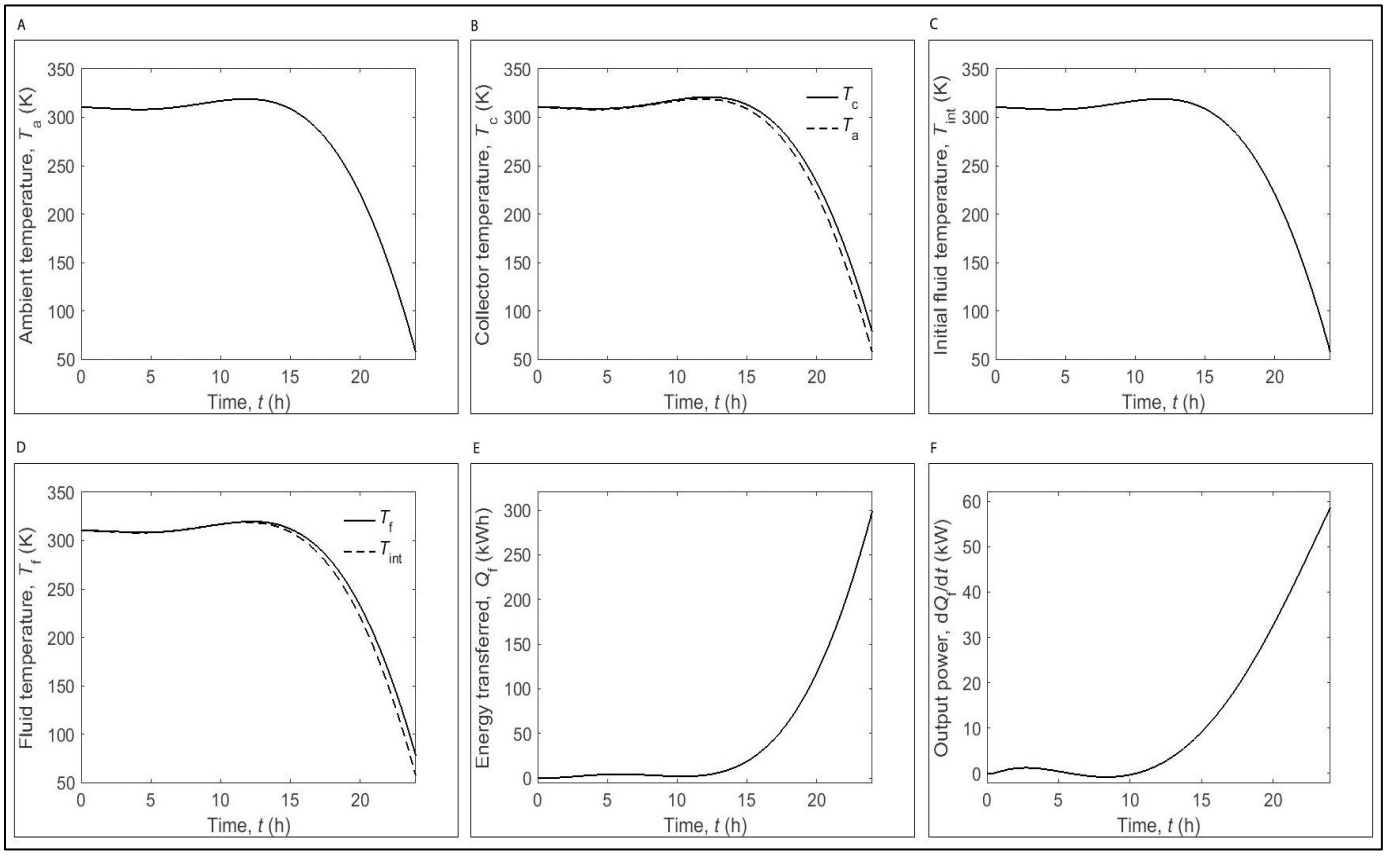
A
Ambient temperature, T_a (K)
Time, t (h)
B
Collector temperature, T_c (K)
T_c
T_a
Time, t (h)
C
Initial fluid temperature, T_{int} (K)
Time, t (h)
D
Fluid temperature, T_f (K)
T_f
T_{int}
Time, t (h)
E
Energy transferred, Q_f (kWh)
Time, t (h)
F
Output power, dQ_f/dt (kW)
Time, t (h)

Tables:

Table.1

Draw solution	Concentration (mol/L)	Osmotic pressure (bar)
NaCl	1.0	47.39
	1.5	73.56
	2.0	101.73
KCl	1.0	44.55
	1.5	67.26
	2.0	90.52
KNO_3	1.0	37.68
	1.5	52.69
	2.0	65.72
KCl+KNO_3	1.0	42.66
	1.5	62.72
	2.0	82.17

Table.2

Collector input data	Value	Unit
Collector surface area (S/A_{sc})	2.32	m^2
Heat loss coefficient (U')	3.97	W/m^2 K
Mass of collector (Mc)	44.0	Kg
Collector heat capacity ($C_{p,c}$)	376.812	J/Kg K
absorptivity coefficient (B)	0.95	
Solar radiation intensity (I_t)	950	W/m^2
Ambient temperature ($T_{a,t}$)		^oK
Collector temperature ($T_{c,t}$)		^oK
heat transfer coefficient of collector (h_c)	734	W/m^2 ^oK
Length of collector (L_c)	2.037	m
fluid flow rate (m_f)	0.6	Kg/s
mass of circulating fluid (M_f)	1000	Kg
flow liquid heat capacity ($C_{p,f}$)	4187	J/kg ^oK
Mass of collector (M_c)	44.0	Kg

Supplementary Information

Collector

The rate of energy entering the collector from irradiation, $\mathrm{d}Q_{\mathrm{Ir}}/\mathrm{d}t$, is given by

$$\frac{\mathrm{d}Q_{Ir}}{\mathrm{d}t} = SBIr \tag{1}$$

since a collector of area S and absorptivity B will absorb at a rate given by the product of these two quantities and the rate of irradiance per unit area, Ir. Similarly, the rate of heat flow from the atmosphere, $\mathrm{d}Q_{\mathrm{a}}/\mathrm{d}t$, is

$$\frac{\mathrm{d}Q_a}{\mathrm{d}t} = SU_1(T_a - T_c) \tag{2}$$

and the rate of heat flow from the fluid, $\mathrm{d}Q_{\mathrm{f,c}}/\mathrm{d}t$, is

$$\frac{\mathrm{d}Q_{c,f}}{\mathrm{d}t} = Sh_c\left(T_f - T_c\right) \tag{3}$$

Summing these contributions gives a total heat flow to the collector of

$$\frac{\mathrm{d}Q_c}{\mathrm{d}t} = S\left(BIr + U_1(T_a - T_c) + h_c\left(T_f - T_c\right)\right) \tag{4}$$

Which, given that the temperature of the collector, T_{c}, is equal to Q_{c} divided by the collector's total heat capacity, $M_{\mathrm{c}}\, C_{\mathrm{p,c}}$, yields

$$\frac{\mathrm{d}T_c}{\mathrm{d}t} = \frac{S}{M_c C_{p,c}}\left(BIr + U_1(T_a - T_c) + h_c\left(T_f - T_c\right)\right) \tag{5}$$

Which may be rearranged to recover the first equation.

Fluid

Making the assumption that the fluid in the collector is perfectly isolated from the atmosphere (i.e. there is no direct heat flow from atmosphere to fluid), this body of fluid can gain or lose energy in two ways: either through the body of the collector or via the fluid entering or leaving the system. These contributions can be written respectively as

$$\frac{\mathrm{d}Q_{f,c}}{\mathrm{d}t} = Sh_c\left(T_c - T_f\right) \tag{6}$$

$$\frac{dQ_{flow}}{dt} = m_{f,c}C_{p,f}\left(T_{int} - T_f\right) \tag{7}$$

The second relation follows from the understanding that the energy per unit mass entering or leaving the system is equal to the product of $C_{p,f}$ and the temperature of the entering/leaving fluid; in turn, the total rate of energy entering or leaving the system in this way is found by multiplying this product by the mass flow rate, $m_{f,c}$. Combining these contributions and noting that the energy entering the system is spread over the total mass Mf of fluid present, the rate of temperature change is given by

$$\frac{\mathrm{d}T_f}{\mathrm{d}t} = \frac{1}{M_f C_{p,f}}\frac{\mathrm{d}Q_f}{\mathrm{d}t} = \frac{1}{M_f C_{p,f}}\left(Sh_c\left(T_c - T_f\right) + m_{f,c}C_{p,f}\left(T_{int} - T_f\right)\right) \tag{8}$$

Which rearranges to the second differential equation given previously.

Decoupling the equations

Next, we need to decouple the two first order ordinary differential equations (ODEs). To do this, we may first differentiate dT_c/dt once more with respect to t to yield the second order ODE,

$$\frac{\mathrm{d}^2T_c}{\mathrm{d}t^2} = A_{11}\frac{\mathrm{d}T_c}{\mathrm{d}t} + A_{12}\frac{\mathrm{d}T_f}{\mathrm{d}t} + B_{11}\frac{\mathrm{d}Ir}{\mathrm{d}t} + B_{12}\frac{\mathrm{d}T_a}{\mathrm{d}t} \tag{9}$$

following which we can substitute for the dT_f/dt term using the other first order ODE. This yields

$$\frac{\mathrm{d}^2T_c}{\mathrm{d}t^2} = A_{11}\frac{\mathrm{d}T_c}{\mathrm{d}t} + A_{12}\left(A_{21}T_c + A_{22}T_f + C_{21}T_{int}\right) + B_{11}\frac{\mathrm{d}Ir}{\mathrm{d}t} + B_{12}\frac{\mathrm{d}T_a}{\mathrm{d}t} \tag{10}$$

and finally

$$\frac{\mathrm{d}^2T_c}{\mathrm{d}t^2} = A_{11}\frac{\mathrm{d}T_c}{\mathrm{d}t} + A_{12}\left(A_{21}T_c + \frac{A_{22}}{A_{12}}\left(\frac{\mathrm{d}T_c}{\mathrm{d}t} - A_{11}T_c - B_{11}Ir - B_{12}T_a\right) + C_{21}T_{int}\right) + B_{11}\frac{\mathrm{d}Ir}{\mathrm{d}t} + B_{12}\frac{\mathrm{d}T_a}{\mathrm{d}t} \tag{11}$$

Where the final step is achieved by rearranging the first order ODE for dT_c/dt to substitute for T_f. Rearranging, one obtains an ODE of the form

$$\frac{\mathrm{d}^2 T_c}{\mathrm{d}t^2} + a\frac{\mathrm{d}T_c}{\mathrm{d}t} + bT_c = g \tag{12}$$

Where

$$\begin{gathered} a = -(A_{11} + A_{22}) \\ b = A_{11}A_{22} - A_{12}A_{21} \\ g = B_{11}\left(\frac{\mathrm{d}Ir}{\mathrm{d}t} - A_{22}Ir\right) + B_{12}\left(\frac{\mathrm{d}T_a}{\mathrm{d}t} - A_{22}T_a\right) + A_{12}C_{21}T_{int} \end{gathered} \tag{13}$$

The MATLAB program proceeds by solving this second order ODE, setting the initial conditions of $T_c(0) = T_a(0)$ and $T_f(0) = T_{int}(0)$, the latter of which yields an condition for the value of $\mathrm{d}T_c/\mathrm{d}t$ at $t = 0$. Inserting the resulting solution for T_c into the first order ODE for T_f, T_f may be subsequently also found. For simplicity, we have approximated *Ir* using an eighth order polynomial; this approximation is plotted as a red line over the Gaussian form of *Ir*.

Total energy transfer to fluid

Once T_f is known, the cumulative energy transfer to the fluid, Q_f, may be calculated as a function of time. The energy q_f imparted to a given mass m_f of fluid passing through the system is described by the formula

$$\frac{\mathrm{d}q_f}{\mathrm{d}(T_f - T_{int})} = C_{p,f}m_f \tag{14}$$

So the rate of energy transfer to flowing fluid is

$$\frac{\mathrm{d}q_f}{\mathrm{d}t} = \int (C_{p,f}m_{f,c})d(T_f - T_{int})' = C_{p,f}m_{f,c}(T_f - T_{int}) + c \tag{15}$$

where *c* is a constant of integration. Integrating with respect to time from zero to *t* gives

$$Q_f = C_{p,f}m_{f,c}\int_0^t (T_f - T_{int})dt' + ct \tag{16}$$

Since Q_f is zero at t = 0, *c* can be assigned a value of zero. Consequently,

$$Q_f = C_{p,f} m_{f,c} \int_0^t \left(T_f - T_{int}\right) dt' \tag{17}$$

The MATLAB program uses this equation to calculate Q_f from the derived form of T_f, and from which it also calculates the variation of the output power dQ_f/dt.

References

[1] L. F. Greenlee, D.F. Lawler, B.D. Freeman, B. Marrot, P. Moulin, Reverse osmosis desalination: water sources, technology, and today's challenges, Water Res. 43 (2009) 2317–2348.
[2] World Economic Forum, The Global Risks Report 2016. Part 1, http://reports. weforum.org/global-risks-2016/part-1-title-tba/?doing_wp_cron=1548994188.4654359817504882812500, (2016).
[3] M. Xie, L. D. Nghiem, W. E. Price, M. Elimelech, A Forward Osmosis−Membrane Distillation Hybrid Process for Direct Sewer Mining: System Performance and Limitations, Environ. Sci. Technol. 47 (2013) 13486−13493.
[4] Q. Ge, M. Ling, et al., Draw solutions for forward osmosis processes: developments, challenges, and prospects for the future, J. Membr. Sci. 442 (2013) 225–237.
[5] S. Sahebi, S. Phuntsho, Y.C. Woo, M.J. Park, L.D. Tijing, S. Hong, H.K. Shon, Effect of sulphonated polyethersulfone substrate for thin film composite forward osmosis membrane, Desalination. 389 (2016) 129–136.

[6] W. A. Suwaileh, D. J. Johnson, S. Sarp, N. Hilal, Advances in forward osmosis membranes: altering the sub-layer structure via recent fabrication and chemical modification approaches, Desalination. 436 (2018) 176–201.

[7] D. J. Johnson, W. A. Suwaileha, A. Mohammed, N. Hilal, Osmotic's potential: an overview of draw solutes for forward osmosis, Desalination. 434 (2018) 100–120.

[8] Q. Ge, J. Su, G.L. Amy, T.-S. Chung, Exploration of polyelectrolytes as draw solutes in forward osmosis processes, Water Res. 46 (2012) 1318–1326.
[9] Sh. Phuntsho, H. K. Shon, T. Majeed, I. El Saliby, S. Vigneswaran, J. Kandasamy, S. Hong, S. Lee, Blended fertilizers as draw solutions for fertilizer-drawn forward osmosis desalination, Environ. Sci. Technol. 46 (2012) 4567−4575.

[10] W. Suwaileh, D. Johnson, N. Hilal, Brackish water desalination for agriculture: Assessing the performance of inorganic fertilizer draw solutions, Desalination. 456 (2019) 53–63.

[11] M. M. Ling, T. S. Chung, Desalination process using superhydrophilic nano- particles via forward osmosis integrated with ultrafiltration regeneration, Desalination. 278 (2011) 194–202.

[12] S. Zhao, L. Zou, D. Mulcahy, Brackish water desalination by a hybrid forward osmosis–nanofiltration system using divalent draw solute, Desalination. 284 (2012)175–181.

[13] S. Bhojwani, K. Topolski, R. Mukherjee, D. Sengupta, M. M. El-Halwagi, Technology review and data analysis for cost assessment of water treatment systems, Sci. Total Environ. 651 (2019) 2749–2761.

[14] N. Ghaffour, T. M. Missimer, G. L. Amy, Technical review and evaluation of the economics of water desalination: current and future challenges for better water supply sustainability, Desalination. 309 (2013) 197–207.

[15] H. D. Raval, P. Koradiya, Direct fertigation with brackish water by a forward osmosis system converting domestic reverse osmosis module into forward osmosis membrane element, Desalination and Water Treatment. 57 (2016) 15740-15747.

[16] N. C. Nguyen, S. S. Chen, H. Y. Yang, N. T. Hau, Application of forward osmosis on dewatering of high nutrient sludge. Bioresour. Technol. 132 (2013) 224−229.

[17] K. Lutchmiah, E. R. Cornelissen, D. J. H. Harmsen, J. W. Post, K. Lampi, H. Ramaekers, L. C. Rietveld, K. Roest, Water recovery from sewage using forward osmosis. Water Sci. Technol. 64 (2011) 1443−1449.

[18] Sh. Zou, H. Yuan, A. Childress, Z. He, Energy consumption by recirculation: A missing parameter when evaluating forward osmosis, Environ. Sci. Technol., 50 (2016) 6827−6829.
[19] C. Tan, H. Ng, A novel hybrid forward osmosis-nanofiltration (FO-NF) process for seawater desalination: draw solution selection and system configuration, Desalination. Water Treat. 13 (2010) 356–361.
[20] A. I. Schafer, A. Broeckmann, B. S. Richards, Renewable energy powered membrane technology. 1. Development and characterization of a photovoltaic hybrid membrane system. Environ. Sci. Technol. 41 (2007) 998−1003.
[21] Y. Zhang, L. Pinoy, A natural driven membrane process for brackish and wastewater treatment: photovoltaic powered ED and FO hybrid system, Environ. Sci. Technol. 47 (2013) 10548–10555.
[22] H. C. Duong, P. Cooper, B. Nelemans, T. Y. Cath, L. D. Nghiem, Optimising thermal efficiency of direct contact membrane distillation by brine recycling for small scale seawater desalination, Desalination. 374 (2015) 1–9.

[23] M. Asghari, A. Harandizadeh, M. Dehghani, H. R. Harami, Persian Gulf desalination using air gap membrane distillation: Numerical simulation and theoretical study, Desalination. 374 (2015) 92–100.[24] W. Suwaileh, D. Johnson, S. Khodabakhshi, N. Hilal, Development of forward osmosis membranes modified by cross-linked layer by layer assembly for brackish water desalination, Journal of Membrane Science. 583 (2019) 267 – 277.
[25] H. Attia, D. J. Johnson, C. J. Wright, N. Hilal, Comparison between dual-layer (superhydrophobic–hydrophobic) and single superhydrophobic layer electrospun membranes for heavy metal recovery by air-gap membrane distillation, Desalination. 439 (2018) 31–45.
[26] A. Altaee, G. Zaragoza, A conceptual design of low fouling and high recovery FO–MSF desalination plant, Desalination. 343 (2014) 2–7.

[27] SchücoSol K. Flat−plate solar collectors http://www.sigenergy.co.uk/documents/SchucoSol%20Solar%20Thermal%20Compact%20Line%20Product%20Information%20Sheet.pdf.

[28] N. T. U. Kumara, A. Martin, Experimental modeling of an air-gap membrane distillation module and simulation of a solar thermal integrated system for water purification, Desalination and Water Treatment. 84 (2017) 123–134.

[29] M. Mulholland, Applied Process Control, First ed., Wiley-VCH Verlag GmbH & Co. KGaA, Germany, 2016.

[30] H. Chang, G. Wang, Y. Chen, Ch. Li, Ch. Chang, Modeling and optimization of a solar driven membrane distillation desalination system, Renewable Energy. 35 (2010) 2714-2722.

[31] E. D. Andersen, 1998, Linear optimization: Theory, methods, and extensions, Odense M, Denmark. Available at: http://citeseerx.ist.psu.edu/viewdoc/download?doi=10.1.1.229.3959&rep=rep1&type=pdf.

[32] Solar radiation in Kuwait Posted on August, 20 in CONGRESS, http://energyprofessionalsymposium.com/?p=5392

[33] A. Achilli, T. Y. Cath, A. E. Childress, Selection of inorganic-based draw solutions for forward osmosis applications, J. Membr. Sci. 364 (2010) 233–241.

[34] Y. Yang, M. Chen, Sh. Zou, X. Yang, T. E. Long, Z. He, Efficient recovery of polyelectrolyte draw solutes in forward osmosis towards sustainable water treatment, Desalination. 422 (2017) 134–141.

[35] N. T. Hau, Sh. Chen, N. C. Nguyen, K. Z. Huang, H. H. Ngo, W. Guo, Exploration of EDTA sodium salt as novel draw solution in forward osmosis process for dewatering of high nutrient sludge, J. Membr. Sci. 455 (2014) 305–311.
[36] M. Ahmed, R. Kumar, Y. Al-Wazzan, B. Garudachari, J. P. Thomas, Assessment of Performance of Inorganic Draw Solutions Tested in Forward Osmosis Process for Desalinating Arabian Gulf Seawater Arabian Journal for Science and Engineering. 43 (2018) 6171–6180.
[37] M. L. Stone, A. D. Wilson, M. K. Harrup, F. F. Stewart, An initial study of hexavalent phosphazene salts as draw solutes in forward osmosis, Desalination. 312 (2013) 130–136.
[38] I. Chaoui, S. Abderafi, S. Vaudreuil, T. Bounahmidi, Water desalination by forward osmosis: draw solutes and recovery methods – review, Environmental Technology Reviews. 8 (2019) 25-46.
[39] Ch. Wang, B. Gao, P. Zhao, R. Li, Q. Yue, H. K. Shon, Exploration of polyepoxysuccinic acid as a novel draw solution in the forward osmosis process, RSC Adv. 7 (2017) 30687–30698.
[40] X. Bao, Q. Wu, W. Shi, W. Wang, H. Yu, Z. Zhu, X. Zhang, Z. Zhang, R. Zhang, F. Cui, Polyamidoamine dendrimer grafted forward osmosis membrane with superior ammonia selectivity and robust antifouling capacity for domestic wastewater concentration, Water Research. 153 (2019) 1-10.
[41] J. R. Werber, A. Deshmukh, M. Elimelech, The Critical Need for Increased Selectivity, Not Increased Water Permeability, for Desalination Membranes, Environ. Sci. Technol. Lett. 3 (2016) 112−120.
[42] B. Mi, M. Elimelech, Gypsum scaling and cleaning in forward osmosis: Measurements and mechanisms, Environ. Sci. Technol. 44 (2010) 2022–2028.
[43] Sh. Zou, Z. He, Enhancing wastewater reuse by forward osmosis with self-diluted commercial fertilizers as draw solutes, Water Research. 99 (2016) 235-243.
[44] M. Elimelech, W.A. Phillip, The future of seawater desalination: energy, technology, and the environment, Science. 333 (2011) 712–717.
[45] N. M. Mazlan, P. Marchetti, H. A. Maples, B. Gu, S. Karan, A. Bismarck, A. G. Livingston, Organic fouling behaviour of structurally and chemically different forward osmosis membranes – A study of cellulose triacetate and thin film composite membranes, Journal of Membrane Science. 520 (2016) 247–261.
[46] E. Guillén-Burrieza, G. Zaragoza, S. Miralles-Cuevas, J. Blanco, Experimental evaluation of two pilot-scale membrane distillation modules used for solar desalination, Journal of Membrane Science. 409– 410 (2012) 264– 275.
[47] F. A. Banat, J. Simandl, Theoretical and experimental study in membrane distillation, Desalination. 95 (1994) 39–52.
[48] M. R. Choudhury, N. Anwar, D. Jassby, Md. S. Rahaman, Fouling and wetting in the membrane distillation driven wastewater reclamation process – A review, Advances in Colloid and Interface Science. 269 (2019) 370–399.
[49] M. Laqbaqbi, J. A. Sanmartino, M. Khayet, C. García-Payo, M. Chaouch, Fouling in Membrane Distillation, Osmotic Distillation and Osmotic Membrane Distillation, Appl. Sci. 7 (2017) 334.

[50] M. Gryta, M. Tomaszewska, K. Karakulski, Wastewater treatment by membrane distillation, Desalination. 198 (2006) 67–73.

[51] A. Alkhudhiri, N. Hilal, Air gap membrane distillation: A detailed study of high saline solution, Desalination. 403 (2017) 179–186.

[52] J. Li, Y. Guan, F. Cheng, Y. Liu, Treatment of high salinity brines by direct contact membrane distillation: Effect of membrane characteristics and salinity, Chemosphere. 140 (2015) 143–149.

[53] S. Srisurichan, R. Jiraratananon, A. G. Fane, Mass transfer mechanisms and transport resistances in direct contact membrane distillation process, Journal of Membrane Science. 277 (2006) 186–194.

[54] A. Boubakri, A. Hafiane, S.A.T. Bouguecha, Direct contact membrane distillation: capability to desalt raw water, Arab. J. Chem. 10 (2017) 3475–3481.

[55] Y. Guan, J. Li, F. Cheng, J. Zhao, X. Wang, Influence of salt concentration on DCMD performance for treatment of highly concentrated NaCl, KCl, $MgCl_2$ and $MgSO_4$ solutions, Desalination. 355 (2015) 110–117.